Journal of Computational Applied Mechanics 2025, 56(2): 424-456

DOI: 10.22059/jcamech.2025.390125.1357

RESEARCH PAPER

Insights of Nonlinear Vibration of Oscillators Linked with Two-Degrees-of-Freedom

Galal M. Moatimid [a], T. S. Amer [b], Mona A. A. Mohamed [a, *], Abdallah A. Galal [c], A. I. Ismail [d]

[a] *Ain Shams University, Department of Mathematics, Faculty of Education, Cairo 11566, Egypt*
[b] *Tanta University, Department of Mathematics, Faculty of Science, Tanta 31527, Egypt*
[c] *Tanta University, Department of Engineering Physics and Mathematics, Faculty of Engineering, Tanta 31734, Egypt*
[d] *Mechanical Engineering Department, College of Engineering and Architecture, Ummul Al Qura University, Makkah, Saudi Arabia*

Abstract

Damped coupled harmonic nonlinear oscillators are essential to model several physical systems, including electrical circuits, mechanical structures, and definite biological systems. Therefore, the current work aims to examine the honest non-perturbative approach (NPA) to get periodic solutions for damped and conservative coupled mass-spring systems with linear and nonlinear stiffness that exhibit nonlinear free vibrations. The NPA is mainly based on the He's frequency formula (HFF). Four practical models of two-degree-of-freedom (TDOF) oscillation systems are demonstrated to display the accuracy, effectiveness, and applicability of the proposed approach. Furthermore, the study intends to achieve approximate solutions for small amplitude parametric factors, without observing the restrictions imposed by traditional perturbation approaches. The method is also extended to reveal ideal solutions for systems of nonlinear coupled oscillators. The iterative approximations of the solutions of parametric nonlinear fluctuations necessitate a quick estimation of the frequency-amplitude relationship. The produced parametric equation is validated using the Mathematica Software (MS), and it exhibits excellent agreement with the numerical solution (NS) of the original system. The achieved responses of the examined models, besides the solutions of two limited cases, are graphically represented. These graphs show the temporal behaviors of these models and reveal a good impact of the acted parameters. The time histories of these solutions show consistent decay behavior, implying the stability of the results. Moreover, the related phase plane curves are displayed in various plots that have spiral curves directed inward at one single point. The behavior of the limited cases has periodicity forms with the variation of several acted parameters. Therefore, the corresponding curves of the phase plane have the forms of symmetric closed curves, i.e., limit cycles are produced. The present methodology seems to be straightforward, promising, powerful, and attractive. It can be employed in several kinds of multi degrees of freedom in dynamical systems.

Keywords: Coupled nonlinear oscillators; Nonlinear stiffness; Damping nonlinear harmonic oscillator; Non perturbative approach; He's frequency formulation.

[*] Corresponding author: Tel. +201114989458. Email Address: monaali@edu.asu.edu.eg

1. Introduction

The nonlinear ordinary differential equations (ODEs) are a compensated subject in engineering, physics, structures, mathematics, and other related fields. Consequently, researchers have widely employed a variety of analytical and numerical methods to examine these issues. Analytical approaches are particularly appealing due to their efficacy in providing a timely and approximate calculation of the frequency of parameters. The process of obtaining exact analytical solutions for nonlinear oscillator problems is often challenging and, in some cases, may prove impossible. There is an increasing emphasis on researching the motion of the TDOF nonlinear oscillation system. The generalized Galerkin's approach is formulated for the holonomic systems with several degrees of freedom. Two autonomous nonlinear TDOF oscillators were used as examples to demonstrate the use of the technology[1]. The nonlinear free vibration of a conservative, coupled mass-spring system with cubic nonlinearity can be solved using two effective analytical approaches: He's Max-Min approach and HFF[2]. The study investigated the analysis of a system comprising two masses with TDOF[3]. The system's behavior was characterized by a set of consistent, highly nonlinear ODEs. It was shown that a limited number of iterations yielded very precise responses that could be applied to a wide range of vibration amplitudes. The equation of motion (EOM) of a two-mass system connected with a cubic nonlinear stiffness can be described analytically using a system of two coupled ODEs with strong cubic nonlinearities[4]. The analytical solutions for this specific category of ODEs were easily accessible. The movement of the masses exhibited a distinct blend of translational and oscillatory motion. The TDOF systems were essential in modeling a range of real physics and engineering vibration modeling systems, including elastic beams complemented by two springs and milling equipment vibration[5]. These systems comprise two second-order nonlinear ODEs. The EOM for a system with multiple DOF can be converted into the equations of the Duffing oscillator (DO) as mentioned earlier[6].

The growing attraction with the DO, a key issue in the nonlinear oscillations, is primarily motivated by its considerable utilization in many physical processes. These examples encompass the pendulum, magneto-elastic mechanical systems, and the process of extracting periodic orbits, and the nonlinear dynamics of materials with minor elasticity. The work utilized the homotopy perturbation method (HPM) and modified the Lindstedt-Poincare approach to examine the nonlinear free vibrations of beams that are simply supported and double-clamped and are subjected to axial loads[7]. The Galerkin decomposition method was employed to convert the EOM, which was dimensionless, into a collection of nonlinear ODEs. The results derived from the instances of the cubic-quintic DO and Duffing-harmonic equation showcased the approach's exceptional precision, straightforwardness, and effectiveness[8]. The methodology can easily be extended to include other nonlinear oscillators. The main goal of several research attempts is to attain more accurate solutions for ODEs by employing either analytical or numerical methods. Accordingly, many works have concentrated on creating rough analytical methods to discover rough solutions for nonlinear ODEs, such as the HPM[9]. To examine the impact of vibrational amplitude on the dynamic pull-in instability of double-sided-actuated nano-torsional switches, research was performed that identified a nonlinear relationship between frequency and amplitude[10]. The HPM was employed to analyze the impact of fundamental parameters on the pull-in instability and natural frequency. The study examined the oscillation of nonlinear nano-electromechanical resonators using a unique analytical approximate technique known as the global residue harmonic balancing approach[11]. The proposed methodology was successfully implemented and evaluated using quantitative measures. An illustrative example demonstrated the validity and feasibility of the technique, which will be expanded upon in more detail. A fundamental summary of the principles underlying the vibrational iteration method was provided[12]. The early exposition of the vibrational iteration approach centered on essential concepts such as the general Lagrange multiplier, restricted variation, and correction function, which are presented in a heuristic manner. The study made a conscious attempt to offer a lucid and instinctive comprehension of the technique. A unique method was proposed to tackle nonlinear problems by integrating the HPM with a traditional perturbation technique[13]. In contrast to conventional perturbation approaches, the proposed technique does not require a small parameter to be present in the equation. The proposed method can effectively influence the advantages of traditional perturbation methodologies. The results indicated that the innovative method was extremely effective and straightforward. The authors presented a novel analytical perturbation methodology to get accurate and well-organized analytical solutions for nonlinear ODEs with high-order nonlinearity[14]. The obtained results were compared to numerical and previously published data, which confirmed the usefulness and correctness of the existing technique. The strategy was found to produce more accurate and computationally efficient results in comparison to other established methods. The study recorded the changing behavior of a novel auto-parametric TDOF system as it encountered exterior torque and force[15]. The many scales technique was employed to obtain the analytical approximation solutions for the equations in this system.

The application of the nonlinear instability concept played a pivotal role in comprehending and predicting complicated atmospheric phenomena, such as hurricanes, tornadoes, and other turbulent weather events. The nonlinear vibrations have a crucial role in disciplines including physics, electrical engineering, and modern manufacturing. They serve as the essential basis for comprehending different nonlinear phenomena. The DO played a pivotal role in this particular case. Their responses depicted a diverse array of natural processes, physical notions, and engineering occurrences. Several suggestions were given about the theoretical aspects of the DO issue. In contrast to the theoretical frameworks of the DO, the method of dampening the DO was highly precise and nearly certain[16]. Therefore, many researchers have attempted to determine the solution. The damped ODE with higher-order nonlinearities was solved utilizing both computational and conceptual methods[17]. The relationship between the frequency and amplitude in this particular scenario can be evaluated by employing the HFF. A study was undertaken to compare HFF and its modifications in terms of residual computation[18]. Effective techniques of residual computation were presented, which can be utilized to accurately establish the frequency of a nonlinear oscillator. The understanding of HFF was essential for the analysis of the other aspects of the prediction results[19]. Although an accurate response could be obtained, there was still an area for additional advancement. The inclusion of considerable nonlinearity of ODEs was designed to showcase the precision of the solution approach. The frequency accuracy was considered exceptional, therefore establishing it as the most direct approach for nonlinear oscillators[20]. The un-damped degree of oscillation was significantly enhanced by the high-frequency force field[21]. The study investigated the precise and thorough determination of the frequency-amplitude ratio for intense or distinct nonlinear oscillations. The NPA has recently been employed in the dynamic system. The NPA has been used in both the disciplines of dynamical systems and EHD stability to conduct stability investigations[22-34]. Because of the challenges in evaluating the DO, this topic has been acknowledged as a critical field of research that requires further investigation to produce more accurate responses. Consequently, in the current study, the utilization of this NPA approach is considered to be adequate. The HFF was employed to investigate nonlinear vibrations in mechanical systems, a crucial basis in the development of robust and dependable mechanical structures and components. The utilization of HFF was applied in the analysis and generation of oscillatory patterns in electrical circuits, particularly those that include nonlinear elements such as semiconductors. It should be noted that the Chinese mathematician Prof. He is known for his expertise in solving nonlinear oscillators. The author introduced a straightforward yet efficient method called HFF[35]. The HFF was employed by numerous writers with remarkable efficacy.

Coupled dynamic systems, which involve the reciprocal influence of multiple interacting organizations, have widespread applications in various fields. Through the analysis of machinery interactions, it enhances both the design and maintenance processes. The design of autos, robotics, and technology is of utmost importance. By modeling the relationships between the ground and the buildings, it improves the structural flexibility of buildings in order to withstand earthquakes. It ensures safety by analyzing the interactions between mechanisms under dynamic stresses. Through the simulation of the interactions between different apparatuses of aircraft and spacecraft, it enhances stability and control. By analyzing the interconnected components of the engine and transmission, it improves efficiency. It simplifies the process of designing medical devices by representing the interactions they have with different regions of the body. Considering the huge importance of the above factors, the current study is conducted. It is widely recognized that technology has the ability to analyze and control oscillations in constructions such as buildings and bridges. Ensuring the stability and comfort of structures is crucial, especially in situations such as earthquakes or heavy traffic. The TDOF system is capable of simulating and controlling the movement of robotic limbs, which often exhibit complex nonlinear dynamics due to their flexible joints and actuators. The method can be utilized to produce devices that convert ambient vibrations into electrical energy. The utilization of the NPA's nonlinear dynamics and stability analysis has the potential to optimize the efficiency of energy gathering equipment. The concepts can be employed to create systems that efficiently isolate buildings or other structures from ground vibrations during seismic events. Through understanding and controlling the complex patterns of motion, it is feasible to create seismic isolation techniques that are more effective. The TDOF systems can analyze and mitigate the dynamic response of platforms and ships when subjected to waves and wind forces, hence enhancing stability and safety. By utilizing the NPA and accurately replicating the nonlinear behavior of systems, engineers, and scientists can develop structures and technologies that are more efficient, stable, and reliable in several domains. To clarify the explanation of the problem, the rest of the paper is structured as follows: A concise explanation of the NPA concerning the interconnected dynamical system is introduced in **§ 2**. Four applications of the connected DO systems and two limited cases of these applications is presented in **§ 3**. Additionally, graphical representations of the obtained results for these systems and their special cases reveal their temporal behaviors and the beneficial impact of the parameters used. The results of time histories show consistent decay behavior, and indicating stability. The associated phase plane curves are shown in several plots. In the limited scenarios, the behavior show periodicity with variations in several applied parameters. So, the phase plane curves appear as symmetric closed loops, indicating the presence of limit cycles with isolated closed curves. In **§ 4**, the achieved results of this work are summarized.

2. Brief Explanation of NPA in Coupled ODEs

This Section concentrates on extending the previous approach of the NPA of a single nonlinear ODE as previously given[22-34]. To accomplish this, we assume a general system of coupled nonlinear ODEs. This system can be articulated in its most fundamental form as follows:

$$\ddot{x}+f_1(x,\dot{x},\ddot{x},y,\dot{y},\ddot{y})+f_2(x,\dot{x},\ddot{x},y,\dot{y},\ddot{y})=f_3(x,\dot{x},\ddot{x},y,\dot{y},\ddot{y}), \tag{1}$$

and

$$\ddot{y}+h_1(y,\dot{y},\ddot{y},x,\dot{x},\ddot{x})+h_2(y,\dot{y},\ddot{y},x,\dot{x},\ddot{x})=h_3(y,\dot{y},\ddot{y},x,\dot{x},\ddot{x}). \tag{2}$$

In this context, f_1 as well as h_1 signify the odd functions that related with the damping forces, f_2 and h_2 represent other odd functions that familiarize extra secular terms. Additionally, f_3 and h_3 are correspond to even functions that do not generate secular relations[35]. Furthermore, x and y point out the coupled dependent-functions of the system. Apart from the damping and restoring forces, the functions f_2 and h_2 indicate even functions. According to the perturbation approaches[35], the odd functions generate secular terms. In contrast, the even functions do not yield any secular relations. For ease of use, the given approach is not significantly distinct from the case of a single linear ODE. As formerly revealed, the objective is to convert the coupled nonlinear as given in Eqs. (1) and (2) into other equivalent linear ones, producing the modest harmonic motion. With respect to the guessing solutions of the given nonlinear ODEs, one reaches

$$u(t)=A\cos\Omega_1 t, \text{ and } v(t)=B\cos\Omega_2 t, \tag{3}$$

where A and B are the initial amplitudes of the equivalent outcomes. Simultaneously, Ω_1 and Ω_2 are the total frequencies which will be determined later.

Eqs. (3) follow the following initial conditions (ICs):

$$u(0)=A,\ \dot{u}(0)=0,\quad v(0)=B, \text{ and } \dot{v}(0)=0. \tag{4}$$

The objective now is to derive the corresponding linear ODEs. To achieve this, we follow the approach outlined in the former studies [22-34] for the single nonlinear ODE. The equivalent damping terms are provided as follows:

$$\left\{\begin{aligned}\sigma_{eqv\,1}&=\int_0^{2\pi/\Omega_1}\dot{u}\,f_1(u,\dot{u},\ddot{u},v,\dot{v},\ddot{v})dt\Big/\int_0^{2\pi/\Omega_1}\dot{u}^2dt=g_1(\Omega_1,\Omega_2),\\ \sigma_{eqv\,2}&=\int_0^{2\pi/\Omega_3}\dot{v}\,h_1(u,\dot{u},\ddot{u},v,\dot{v},\ddot{v})dt\Big/\int_0^{2\pi/\Omega_3}\dot{v}^2dt=g_2(\Omega_1,\Omega_2)\end{aligned}\right.. \tag{5}$$

It is significance to highlight that the functions g_1, and g_2 include all the factors that are originate the functions f_1 and h_1 of the unidentified frequencies.

Conversely, the corresponding frequencies can be determined as follows:

$$\left\{\begin{aligned}\varpi^2_{eqv\,1}&=\int_0^{2\pi/\Omega_1}u\,f_2(u,\dot{u},\ddot{u},v,\dot{v},\ddot{v})dt\Big/\int_0^{2\pi/\Omega_1}u^2dt=g_3(\Omega_1,\Omega_2),\\ \varpi^2_{eqv\,2}&=\int_0^{2\pi/\Omega_2}v\,h_2(u,\dot{u},\ddot{u},v,\dot{v},\ddot{v})dt\Big/\int_0^{2\pi/\Omega_2}v^2dt=g_4(\Omega_1,\Omega_2).\end{aligned}\right. \tag{6}$$

The functions g_3, and g_4 summarize all the parameters that execute the functions f_2 and h_2, and the undetermined natural frequencies contained within it.

Regarding the quadratic functions f_3 and h_3 the corresponding terms signify the non-homogeneous portion. As formerly shown, for a single equation[22-34], these non-homogeneous parts can be established through the following direct substitutions:

Replace: $$u\to\frac{A}{2\sqrt{2}},\dot{u}\to\frac{A\Omega_1}{2\sqrt{2}},\ddot{u}\to\frac{A\Omega_1^2}{2\sqrt{2}},v\to\frac{B}{2\sqrt{2}},\dot{v}\to\frac{B\Omega_2}{2\sqrt{2}}, \text{ and } \ddot{v}\to\frac{B\Omega_2^2}{2\sqrt{2}}.$$

The non-homogeneous parts of the linear ODEs may be established as follows:

$$\begin{cases} \Lambda_1 = f_3\left(\dfrac{A}{2\sqrt{2}}, \dfrac{A\Omega_1}{2\sqrt{2}}, \dfrac{A\Omega_1^2}{2\sqrt{2}}, \dfrac{B}{2\sqrt{2}}, \dfrac{B\Omega_2}{2\sqrt{2}}, \dfrac{B\Omega_2^2}{2\sqrt{2}}\right), \\ \Lambda_2 = h_3\left(\dfrac{A}{2\sqrt{2}}, \dfrac{A\Omega_1}{2\sqrt{2}}, \dfrac{A\Omega_1^2}{2\sqrt{2}}, \dfrac{B}{2\sqrt{2}}, \dfrac{B\Omega_2}{2\sqrt{2}}, \dfrac{B\Omega_2^2}{2\sqrt{2}}\right). \end{cases} \tag{7}$$

Eventually, the related linear ODEs to Eqs. (1) and (2) may be indicated as follows:

$$\ddot{u} + \sigma_{eqv1}\dot{u} + \varpi_{eqv1}^2 u = \Lambda_1, \tag{8}$$

In accordance with the conventional normal form, the middle term in Eq. (8) may be eliminated via the following transformation:

$$u(t) = G_1(t) Exp(-\sigma_{eqv1} t / 2), \tag{9}$$

where $G_1(t)$ is an arbitrary function.

It will be evaluated via the linear ODE as provided in Eq. (8) as follows:

$$\ddot{G}_1 + \Omega_1^2 G_1 = \Lambda_1 Exp(\sigma_{eqv1} / 2), \tag{10}$$

where
$$\Omega_1^2 = \varpi_{eqv1}^2 - \frac{1}{4}\sigma_{eqv1}^2, \tag{11}$$

which denotes the square of the total frequency of the first linear ODE.

Supplementary, the stability criteria are assessed through the following:

$$\Omega_1^2 > 0, \text{ and } \sigma_{eqv1} > 0. \tag{12}$$

Applying the same reasoning formerly outlined, the second linear ODE can be stated as:

$$\ddot{v} + \sigma_{eqv2}\dot{v} + \varpi_{eqv2}^2 v = \Lambda_2. \tag{13}$$

As formerly expounded the parameters σ_{eqv2} and ϖ_{eqv2}^2 are evaluated as outlined in Eqs. (5) and (6).

The integration is performed over the specified interval $0 \to 2\pi/\Omega_2$.

Once again, the middle term in Eq. (13) can be disregarded by applying the following normal form:

$$v(t) = G_2(t) Exp(-\sigma_{eqv2} t / 2). \tag{14}$$

The unknown function $G_2(t)$ is calculated as:

$$\ddot{G}_2 + \Omega_2^2 G_2 = \Lambda_2 Exp(\sigma_{eqv2} t / 2), \tag{15}$$

where
$$\Omega_2^2 = \varpi_{eqv2}^2 - \frac{1}{4}\sigma_{eqv2}^2, \tag{16}$$

which denotes the square of the total frequency of the second linear ODE.

Additionally, the stability restrictions are assessed utilizing the following:

$$\Omega_2^2 > 0, \text{ and } \sigma_{eqv2} > 0. \tag{17}$$

In this context, it's significant to note that the total frequencies Ω_1 and Ω_2 are determined employing the MS during the execution of the *FindRoot* command for the coupled Eqs. (11) and (16).

3. Applications

Two practical of TDOF oscillation systems are provided in this section to demonstrate the applicability, precision, and efficacy of the suggested methodology.

3.1 Example (1): Damped Coupled Harmonic Oscillators

A damped coupled harmonic oscillator is a physical system with two or more masses linked by springs and subjected to damping forces that waste energy. Coupled ODEs that considered the interactions between the masses, the restoring forces from the springs, and the damping forces may be used to describe this system. Damped coupled harmonic oscillators are utilized to model several physical systems, counting electrical circuits, mechanical structures, and definite biological systems. Understanding the dynamics of these systems is essential for scheming stable and efficient structures for devices. Consider a two equal masses system model as explored in Fig. 1, where x and y represent the motion's directions of two equal masses m. Furthermore, b is the damped coefficient, k_1

and k_2 are the stiffness of the spring.

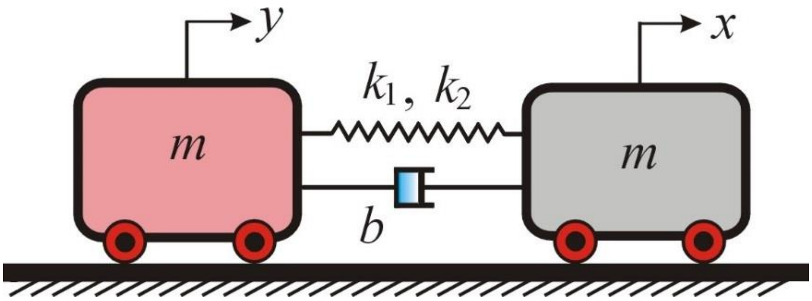

Fig. 1: Two masses connected by linear and nonlinear damped stiffness.

The GOM of the above-described damped coupled harmonic oscillator can be derived by means of the Newton's second law and taking the forces acting on each mass into consideration as follows[2]:

$$\begin{cases} m\ddot{x} = -b(\dot{x}-\dot{y}) - k_1(x-y) - k_2(x-y)^3 \\ m\ddot{y} = -b(\dot{y}-\dot{x}) - k_1(y-x) - k_2(y-x)^3. \end{cases} \tag{18}$$

Eqs. (18) could be written as:

$$\begin{cases} \ddot{x} + \dfrac{b}{m}(\dot{x}-\dot{y}) + \dfrac{k_1}{m}(x-y) + \dfrac{k_2}{m}(x-y)^3 = 0 \\ \ddot{y} + \dfrac{b}{m}(\dot{y}-\dot{x}) + \dfrac{k_1}{m}(y-x) + \dfrac{k_2}{m}(y-x)^3 = 0, \end{cases} \tag{19}$$

The suggested ICs of Eq. (19) are usually written as:

$$x(0) = A,\, y(0) = B,\, \dot{x}(0) = 0, \text{and } \dot{y}(0) = 0. \tag{20}$$

Eqs. (19) could be re-written as:

$$\begin{cases} \ddot{x} + F_1(\dot{y},\dot{x}) + F_2(x,y) = 0 \\ \ddot{y} + F_3(\dot{y},\dot{x}) + F_4(x,y) = 0, \end{cases} \tag{21}$$

where

$$\begin{cases} F_1(\dot{y},\dot{x}) = \dfrac{b}{m}(\dot{x}-\dot{y}), \\ F_2(x,y) = \dfrac{k_1}{m}(x-y) + \dfrac{k_2}{m}(x-y)^3, \\ F_3(\dot{y},\dot{x}) = \dfrac{b}{m}(\dot{y}-\dot{x}), \\ F_4(x,y) = \dfrac{k_1}{m}(y-x) + \dfrac{k_2}{m}(y-x)^3. \end{cases} \tag{22}$$

The trial solutions of the system are assumed in the following form:

$$u = A\cos\Omega_1 t, v = B\cos\Omega_2 t\ , \tag{23}$$

where A and B characterize the initial amplitudes of the equivalent solutions, whereas Ω_1 and Ω_2 are the total frequencies to be determined later.

The functions u and v satisfy the equivalent system:

$$\begin{cases} \ddot{u} + \mu_1\dot{u} + \omega_1^2 u = 0 \\ \ddot{v} + \mu_2\dot{v} + \omega_2^2 v = 0. \end{cases} \tag{24}$$

Through the examination of this system, one can predict that the solutions' behaviors for their equations have decaying manners during the investigated time interval. The parameters ω_1, ω_2 and μ_1, μ_2 are known by equivalent frequencies and equivalent damping, (see Appendix).

(i) The Equivalent Frequencies

To calculate the equivalent frequency, the HFF method can be used with the odd terms $F_2(x, y)$ and $F_4(x, y)$ as:

$$\omega_1^2 = \int_0^{2\pi/\Omega_1} uF_2(u,v)\,dt \Big/ \int_0^{2\pi/\Omega_1} u^2 dt \,. \tag{25}$$

$$\omega_2^2 = \int_0^{2\pi/\Omega_2} vF_4(u,v)\,dt \Big/ \int_0^{2\pi/\Omega_2} v^2 dt \,. \tag{26}$$

(ii) The Equivalent Damping

The HFF allows for the calculation of the equivalent frequency by applying the odd terms $F_1(\dot{y}, \dot{x})$ and $F_3(\dot{x}, \dot{y})$ with

$$\mu_1 = \int_0^{2\pi/\Omega_1} \dot{u}\, F_1(\dot{u},\dot{v})\,dt \Big/ \int_0^{2\pi/\Omega_1} \dot{u}^2\, dt \,. \tag{27}$$

$$\mu_2 = \int_0^{2\pi/\Omega_2} \dot{v}\, F_3(\dot{u},\dot{v})\,dt \Big/ \int_0^{2\pi/\Omega_2} \dot{v}^2\, dt \,. \tag{28}$$

To this end, it should be mentioned that the equivalent frequencies ω_1 and ω_2 as well as the equivalent damping coefficients μ_1 and μ_2 are evaluated via the MS, and due to their complicated formulae, to follow the paper easy, these forms are moved to the Appendix.

Assume the following standard normal forms:

$$u(t) = U(t) Exp(-\mu_1 t / 2) \,. \tag{29}$$

$$v(t) = V(t) Exp(-\mu_2 t / 2) \,. \tag{30}$$

Consequently, substituting Eqs. (29) and (30) into Eqs. (24), one gets:

$$\ddot{U}(t) + \Omega_1^2 U(t) = 0 \,, \tag{31}$$

and

$$\ddot{V}(t) + \Omega_2^2 V(t) = 0 \,, \tag{32}$$

where

$$\Omega_1^2 = \omega_1^2 - \mu_1^2 / 4. \tag{33}$$

$$\Omega_2^2 = \omega_2^2 - \mu_2^2 / 4 \,. \tag{34}$$

We would like to emphasize that the nonlinear ODEs described in Eqs. (19) are expressed as alternating linear equations in Eqs. (24). For the purpose of comparing these two systems, the MS is employed alongside the *(NDSolve)* command; an example of the included factors is shown below.

$$k_3 = 0.5, k_4 = 0.5, b_1 = 0.3, m_1 = 5, A_1 = 0.1, \text{ and } B_1 = -0.1$$

Consequently, Figs. 2 and 3 are provided to depict the solutions for the primary system (19) and the outcomes of the equivalent system outlined in Eq. (24). The solution of the original system (19) is displayed by the solid blue curve, and the dotted red curve represents the NPA solution of the ODEs outlined in Eq. (24). These figures are presented to compare the two solutions mentioned above over 50-time. It is confirmed that the two curves are approximately identical. Infinitesimal absolute errors between the original and the NPA solutions are attained, whereas for the x oscillator the absolute error is 0.00239212 and for the y oscillator, the absolute error is 0.0016253. The same convergence is achieved also through the tables 1 and 2.

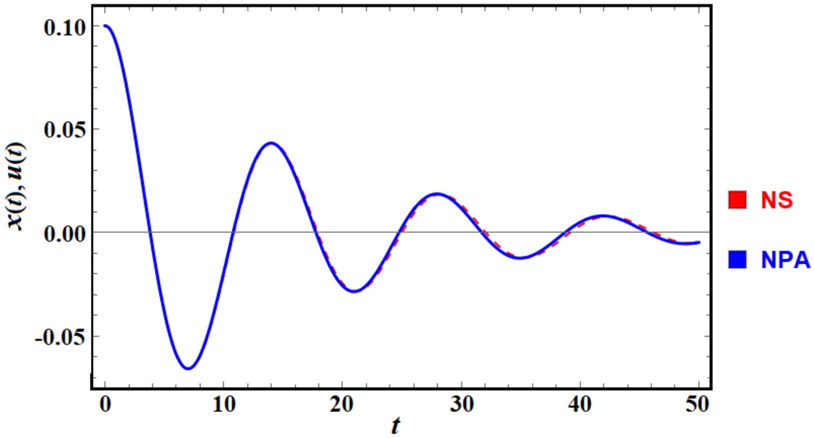

Fig. 2: Illustrates the agreement between the solutions of the nonlinear dynamical system (19) and those of the NPA system (24) for the x oscillator.

Table 1: Verifies the convergence of the real and NPA solutions for the x oscillator.

t	Real x oscillator	Approximate oscillator	Absolute error
0	0.1	0.1	0.0
5	-0.0385328	-0.0387693	0.000236582
10	-0.0200931	-0.0188779	0.00121517
15	0.0395859	0.0388298	0.000756089
20	-0.0245173	-0.0257191	0.00120175
25	0.000188522	0.00258065	0.00239212
30	0.0133053	0.0117232	0.00158217
35	-0.0119756	-0.0123112	0.000335515
40	0.00337248	0.00500392	0.00163145
45	0.00356784	0.00210947	0.00145837
50	-0.00503036	-0.00470779	0.000322569

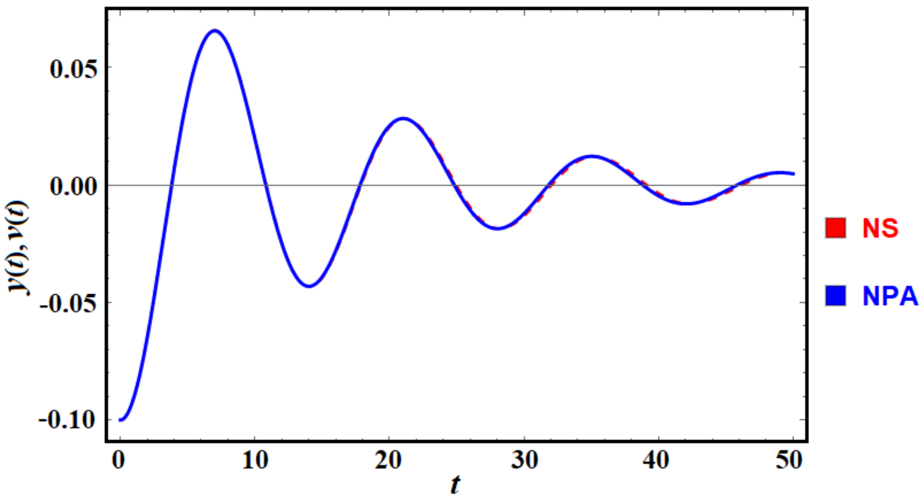

Fig. 3: Shows the agreement between the solutions of the nonlinear dynamical system (19) and those of the NPA system (24) for the y oscillator.

In the comparison of curves generated from linear and nonlinear ODEs, the term consistency generally pertains to the degree to which the behavior or solutions of the nonlinear system correspond with those of the linear system under specific conditions. Linear ODE typically characterizes system where the interaction between variables is directly proportional, yielding predictable, smooth trajectories. Conversely, nonlinear ODE can provide more intricate and unpredictable behavior, including bifurcations or chaotic patterns. In certain instances (e.g., minor disturbances near equilibrium points), the nonlinear curve may closely match or exhibit behavior comparable to the linear curve, demonstrating local consistency. The disparity between the curves amplifies as nonlinear factors gain prominence.

Table 2: Verifies the convergence of the real and NPA solutions for the y oscillator.

t	Real y oscillator	Approximate oscillator	Absolute error
0	-0.1	-0.1	0.0
5	0.0385328	0.03829	0.000242752
10	0.0200931	0.0195873	0.000505719
15	-0.0395859	-0.0390481	0.000537756
20	0.0245173	0.0252238	0.00070652
25	-0.000188522	-0.00181382	0.0016253
30	-0.0133053	-0.0121666	0.00113876
35	0.0119756	0.0122023	0.000226612
40	-0.00337248	-0.00456572	0.00119324
45	-0.00356784	-0.00248824	0.00107959
50	0.00503036	0.00479674	0.00023362

The solutions of the system of Eqs. (24) using the NPA are graphically represented in Figs. 4-9, when the considered values of the parameters are used. These graphs are calculated when the parameters have various values, i.e., $A(=0.1, 0.3, 0.6)$, $B(=-0.1, 0.2, 0.7)$, $b(=0.3, 0.6, 1)$, $k_1(=0.5, 1, 2)$, $k_2(=0.5, 1.5, 2.5)$, and $m(=1, 3, 5)$, respectively. It must be mentioned that portions (*a*) and (*b*) represent the time-dependent solutions u and v for the system of Eqs. (24), where parts (*c*) and (*d*) reveal the related phase plane plots of these solutions. By closely examining the time history curves in parts (*a*) and (*b*), it becomes evident that these curves decay throughout the time interval, as anticipated. This behavior is due to the presence of damping terms in the system. Additionally, it is observed that the rate of decay of the plotted curves changes according to the influencing parameter, as seen in parts (*a*) and (*b*). However, this rate becomes faster for the curves in part (*b*) than the drown ones in part (*a*). Meanwhile, the phase plane curves take on spiral forms that converge to a fixed point, as seen in parts (*c*) and (*d*). These forms vary according to the influencing parameters.

The decaying curves generally refer to the observation that the amplitude of the oscillations or the values of the variables in the system decreases over time. This decay typically indicates the presence of the damping terms $\mu_1\dot{u}$ and $\mu_2\dot{v}$ in the system that given in Eqs. (24), which gradually cause the system's energy to dissipate over time, leading to a decrease in amplitude. These curves often suggest that the system is stable and will eventually settle into a steady state or equilibrium position. The analysis of the phase plane plots in portions (c) and (d) shows that decaying trajectories typically spiral inward towards a fixed point, indicating that the system is moving towards a stable equilibrium.

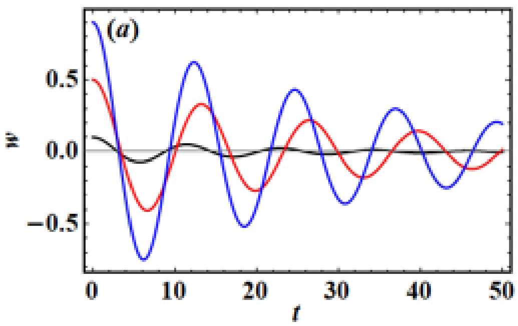

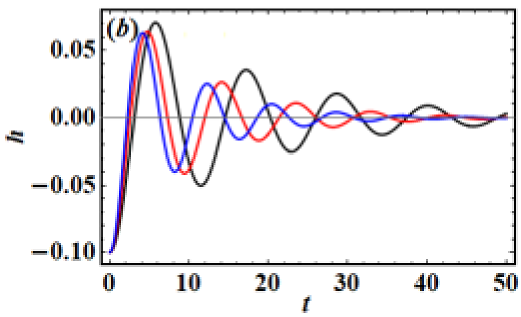

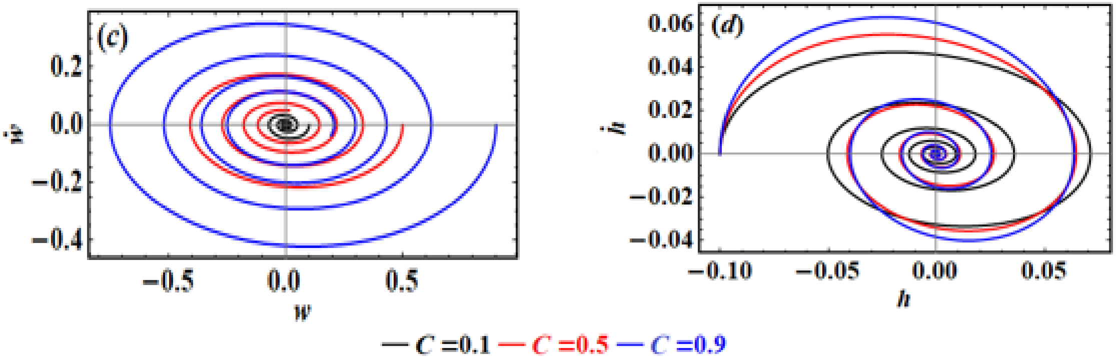

Fig. 4: Displays the behavior of the obtained solutions of system (24) using the NPA and the corresponding phase plane plots at $A(=0.1,0.3,0.6)$.

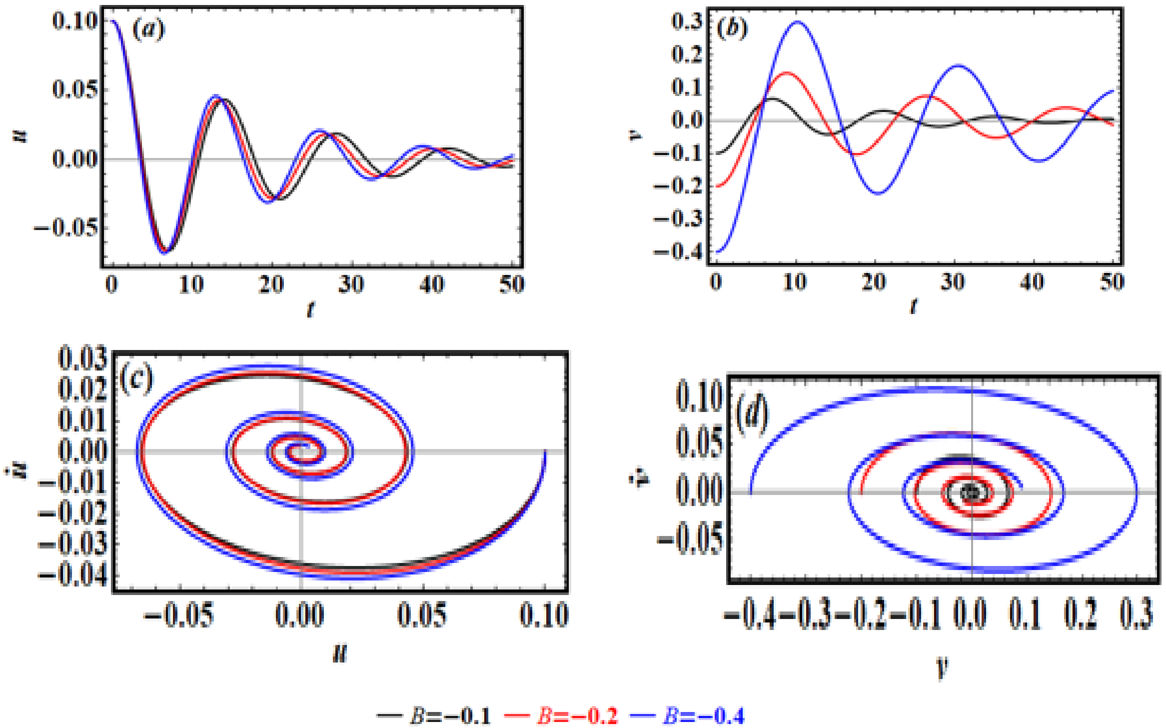

Fig. (5): Illustrates the time variation of u and v of system (24) using the NPA and the related phase plane plots at $B(=-0.1,-0.2,-0.4)$.

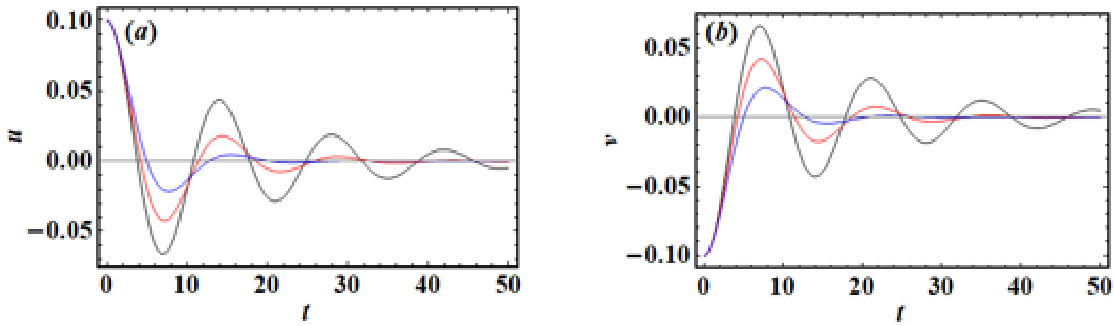

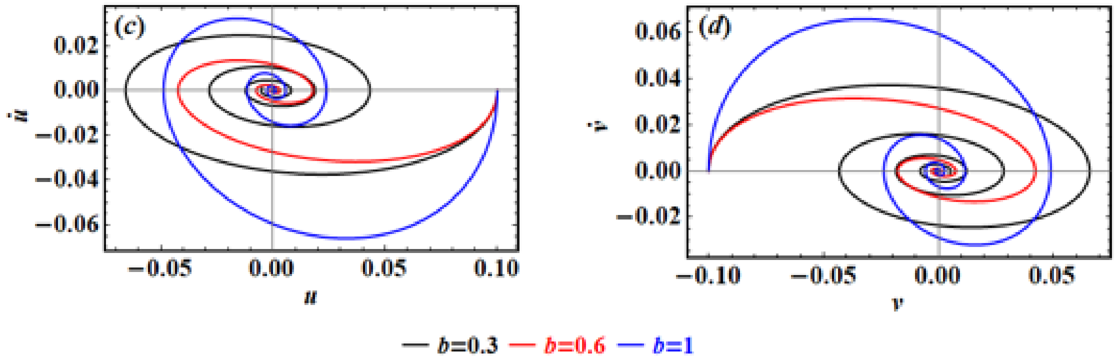

Fig. 6: Displays the solutions' time dependent of system (24) applying the NPA and their related phase plane plots at $b(=0.3, 0.6, 1)$.

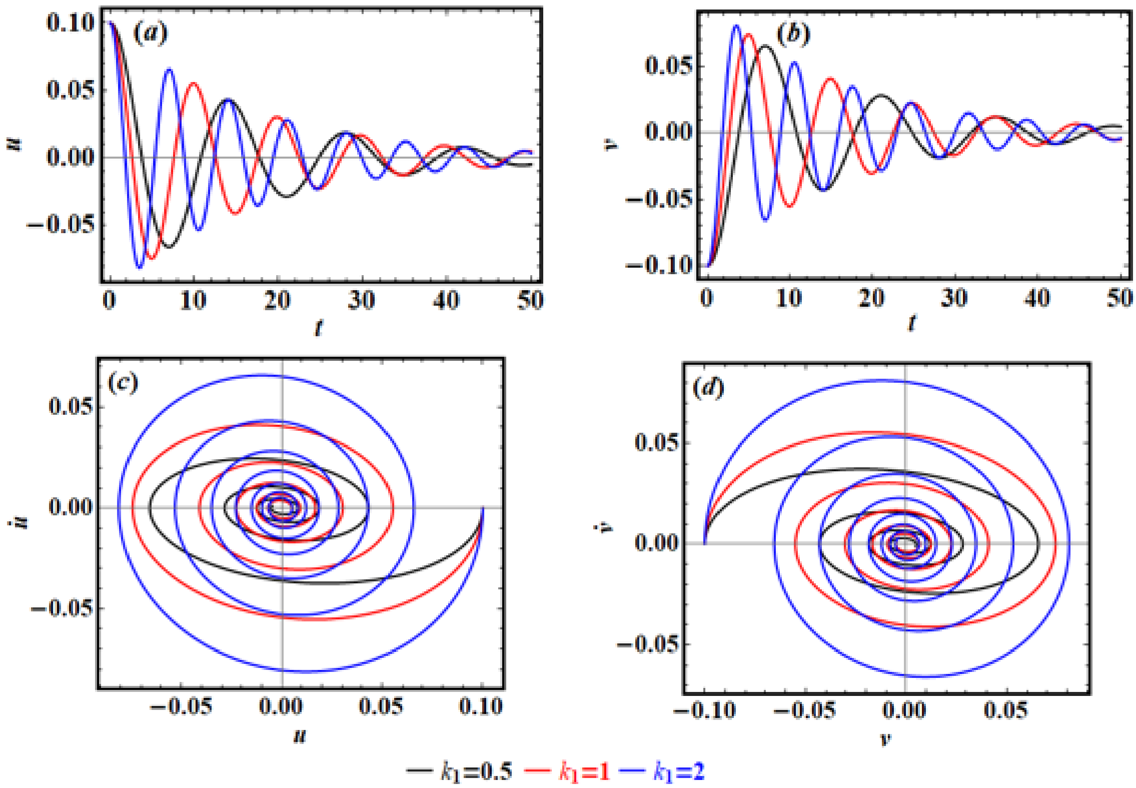

Fig. 7: Displays the temporal behaviors of the functions u and v for the system (24) utilizing the NPA and the related phase plane plots at $k_1(=0.5, 1, 2)$.

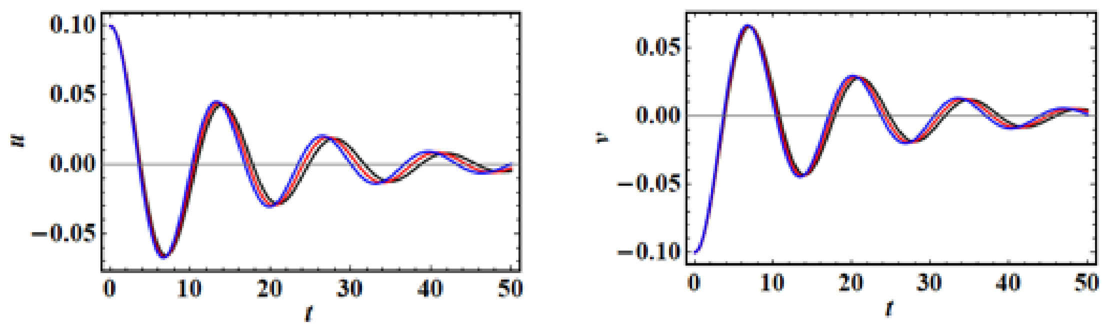

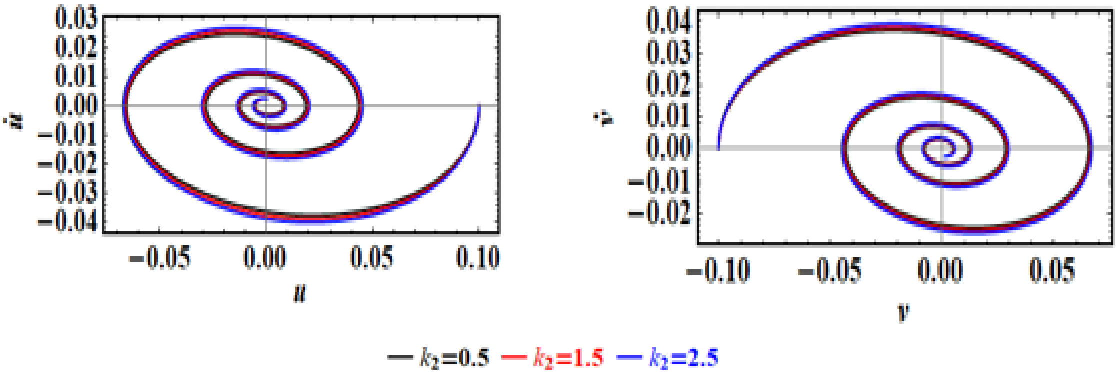

Fig. 8: Displays the behavior of $u(t)$ and $v(t)$ for the system (24) and the related phase plane plots when the NPA is used at $k_2(=0.5,1.5,2.5)$.

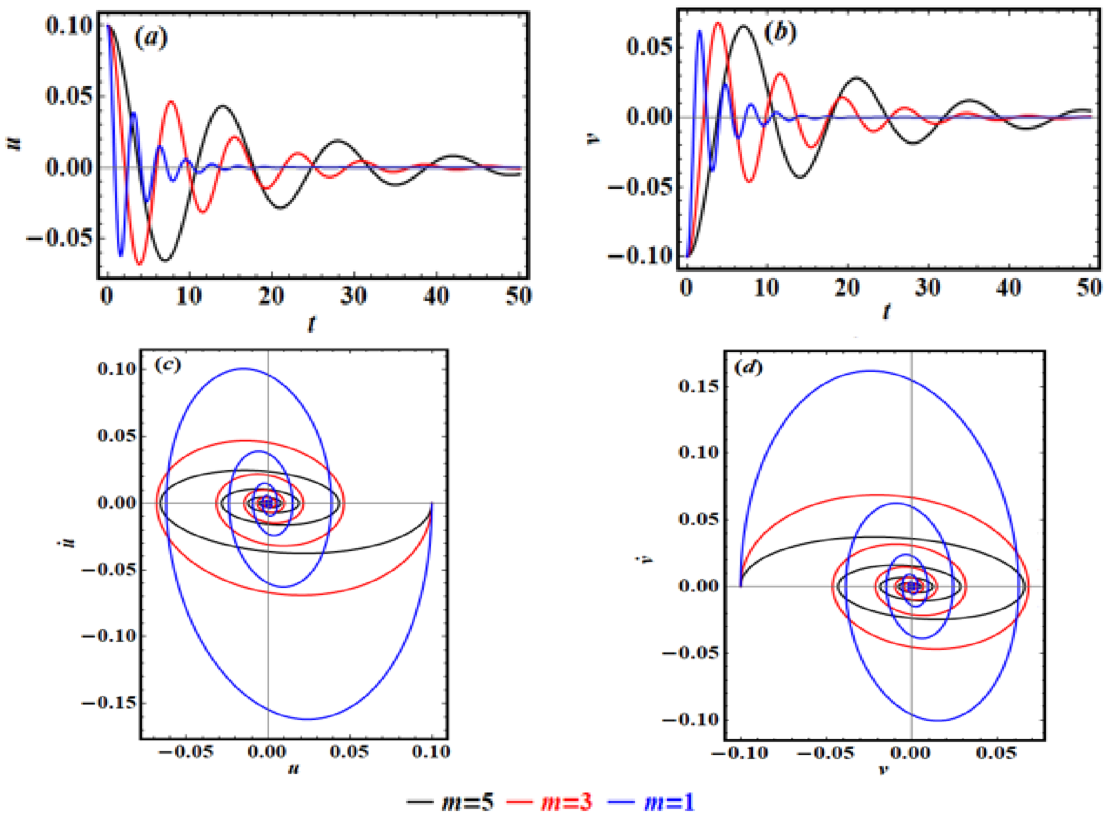

Fig. 9: Displays the waves $u(t)$ and $v(t)$ for the system (24) and their related phase plane curves when the NPA is applied at $m(=1,3,5)$.

3.2 Example (2): Non-Damped Coupled Harmonic Oscillator

Examining the conservative state of the coupled system as given in Eqs. (19), when the damping forces' influences vanish ($b=0$). The coupled harmonic oscillator (19) without damping is expressed as follows [2]:

$$\begin{cases} \ddot{x}+\dfrac{k_1}{m}(x-y)+\dfrac{k_2}{m}(x-y)^3=0 \\ \ddot{y}+\dfrac{k_1}{m}(y-x)+\dfrac{k_2}{m}(y-x)^3=0. \end{cases} \tag{35}$$

Eqs. (35) could be re-written as:

$$\begin{cases} \ddot{x} + F_2(x, y) = 0 \\ \ddot{y} + F_4(x, y) = 0 \end{cases}, \tag{36}$$

where $F_2(x, y)$ and $F_4(x, y)$ are the same functions that were defined before through Eqs. (22).

The trial solutions of the system as given in Eqs. (35) are assumed in the following form:

$$u_1 = A_1 \cos \delta_1 t, v_1 = B_1 \cos \delta_2 t\ , \tag{37}$$

where A_1 and B_1 signify the amplitudes of the equivalent solutions, whereas δ_1 and δ_2 are the total frequencies in this case and they will be determined later.

The functions u_1 and v_1 satisfy the equivalent system:

$$\begin{cases} \ddot{u}_1 + \delta_1^2 u_1 = 0 \\ \ddot{v}_1 + \delta_2^2 v_1 = 0 \end{cases}, \tag{38}$$

where the equivalent frequencies which are considered as the total frequencies in this case can be calculated utilizing the HFF and by using the odd terms $F_2(x, y)$ and $F_4(x, y)$ as:

$$\delta_1^2 = \int_0^{2\pi/\delta_1} u_1 F_2(u,v)\, dt \Big/ \int_0^{2\pi/\delta_1} u_1^2 dt\,. \tag{39}$$

$$\delta_2^2 = \int_0^{2\pi/\delta_2} v_1 F_4(u,v)\, dt \Big/ \int_0^{2\pi/\delta_2} v_1^2 dt\,. \tag{40}$$

These integrals are calculated by MS and their values are equal to their correspondence ω_1 and ω_2 in the previous case which are defined in the Appendix.

Following the same previous procedure when b vanishes and by plotting the solutions of the nonlinear and the equivalent linear equations a very convergence is found between the two solutions. Using the data $k_1 = 0.5, k_2 = 0.5, b = 0, m = 5, A_1 = 0.1, B_1 = -0.1$, the absolute error equals 0.000844 for the x oscillator and equals 0.00667 for the y oscillator, as seen in Figs. 10 and 11, respectively.

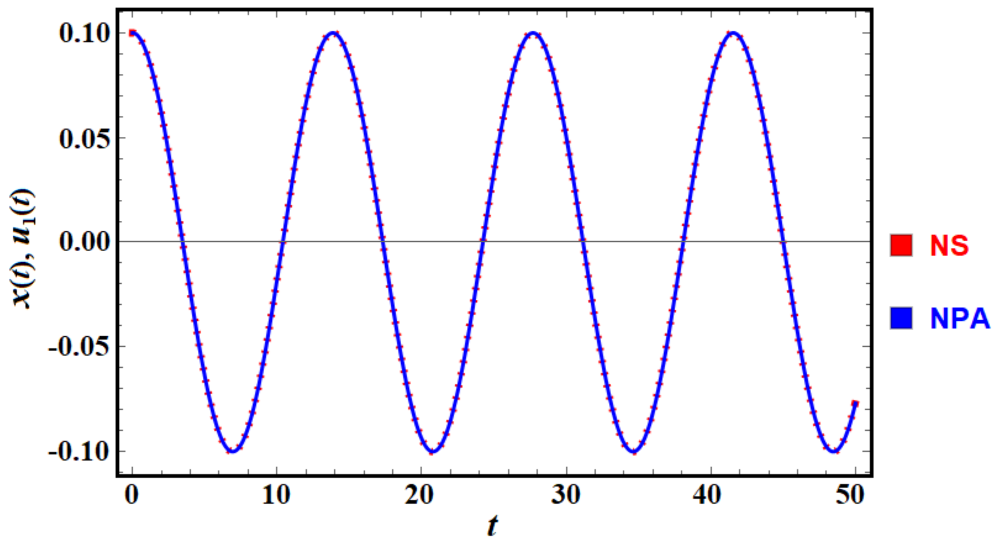

Fig. 10: Demonstrates how the solutions of the nonlinear dynamical system (35) match with those of the NPA linear system for the x oscillator

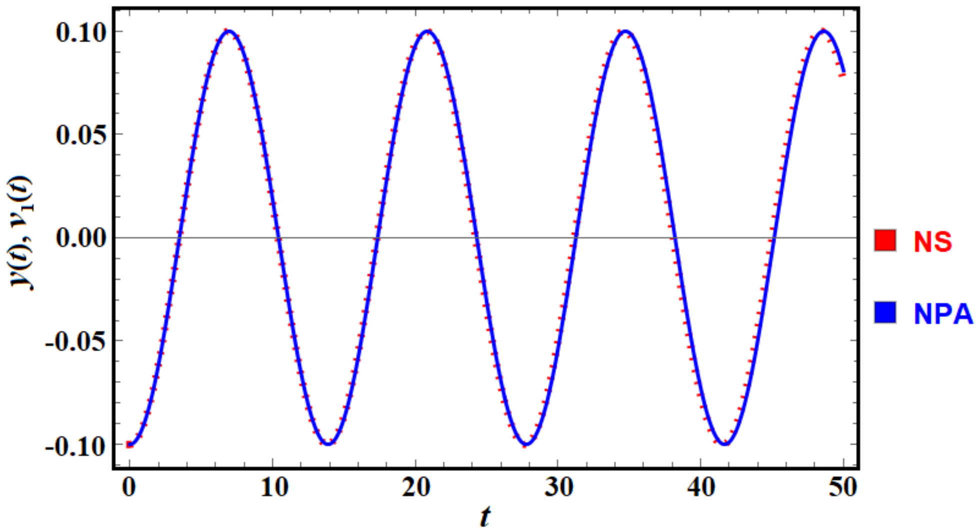

Fig. 11: Depicts how the solutions of the nonlinear dynamical system (35) match with those of the NPA linear system for the y oscillator.

In comparing curves produced by linear and nonlinear ODEs, the term consistency typically refers to the extent to which the behavior or solutions of the nonlinear system align with those of the linear system under particular conditions. Linear ODE often characterizes systems where the interaction between variables is exactly proportional; resulting in predictable, smooth paths. In contrast, nonlinear ODE can exhibit more complex and unpredictable behavior, including bifurcations or chaotic patterns. In specific cases (e.g., modest perturbations around equilibrium points), the nonlinear curve may closely resemble or display behavior akin to the linear curve, indicating local consistency. The divergence between the curves increases as nonlinear components become more significant.

The NPA of the system of Eq. (35) can be easily obtained in view of the analysis of section 3.1, in which they are graphed in Figs. 12,13,14,15, and 16 when the parameters A_1, k_1, k_2, and m have the aforementioned values. These graphs demonstrate that the time-dependent behaviors of the solutions are detailed in portions (*a*) and (*b*) of these figures, and the corresponding phase plane diagrams are provided in parts (*c*) and (*d*). Inspecting the time history waves, it becomes evident that these waves possess periodic forms throughout the whole duration. The graphs show that the oscillation numbers for both solutions u_1 and v_1 differ depending on the parameters in effect. Specifically, the wavelengths and amplitudes of the waves in Fig. 12a diminish as the amplitude parameter A_1 increases for the solution u_1. Conversely, the amplitudes of the waves for the solution v_1 remain stable, while the number of vibrations increases moderately with higher A_1 values, as depicted in Fig. 12b. Based on this analysis, one can say that a good understanding of periodic solutions helps in designing and controlling systems. For example, in mechanical systems, engineers can exploit periodic behavior to improve system performance or to design systems that operate efficiently at desired frequencies. In the $u_1\dot{u}_1$ and $v_1\dot{v}_1$ planes, the related plots depict the relationship between the solutions and their first derivatives, excluding the time parameter. These plots have symmetric closed curves around their vertical or horizontal axes, providing insight into the stability or steady-state behaviors of the solutions, as illustrated in Figs. 12*c* and 12*d*. It must be stated that when the trajectory repeatedly follows a closed curve, it suggests that the system returns to the same state after each period, demonstrating stability. Curves of Figs. 13a and 13b show the time history variation of the solutions u_1 and v_1, respectively, when $B_1 (= -0.1, 0.1, 0.4)$. The graphed curves have periodic forms for any value of B_1. The curves of the phase plane of these solutions have been explored in Figs. 13c and 13d.

The curves in Figs. 14*a* and 14*b* illustrate how the time-dependent functions u_1 and v_1 vary as the parameter k_1 changes. Although the amplitudes of these curves remain constant, the number of fluctuations increases with higher k_1 values, indicating a reduction in wavelength. Consequently, symmetric closed curves are plotted in Figs. 14*c* and 14*d*, each showing three closed curves that may represent one limit cycle per k_1 value. This demonstrates that the solutions are stable and devoid of chaotic behavior with changes in k_1. The variation of the time-dependent functions for the same solutions with changing k_2 is shown in the curves of Figs. 15*a* and 15*b*. The amplitudes of these curves and the number of fluctuations do not vary, with the increase in k_2 values. This can be attributed to the fact that these curves have closer configurations. By excluding time t from the solutions and their first derivatives, closed curves are depicted in Figs. 15*c* and 15*d*.

Figs. 16*a* and 16*b* display how the functions $u_1(t)$ and $v_1(t)$ vary with mass values of $1, 3,$ and 5. The data clearly indicate that changes in mass parameters significantly affect the periodic wave behavior, confirming that the number of oscillations decreases as mass increases. Thus, as the mass m increases, the wavelengths of the plotted waves grow, while the amplitudes remain constant. The phase plane plots in Figs. 16*c* and 16*d*, which illustrate three distinct closed curves for varying mass values, demonstrate that the motion of the examined system remains stable throughout the entire time interval.

Overall, periodic solutions mean that the system behavior is predictable over time. If a system exhibits periodic behavior, you can anticipate its future states based on its current state, which is valuable for both theoretical analysis and practical applications. Moreover, closed symmetric curves in phase plane plots provide a clear and valuable picture of a system's periodic behavior, stability, and energy characteristics, aiding both theoretical analysis and practical applications.

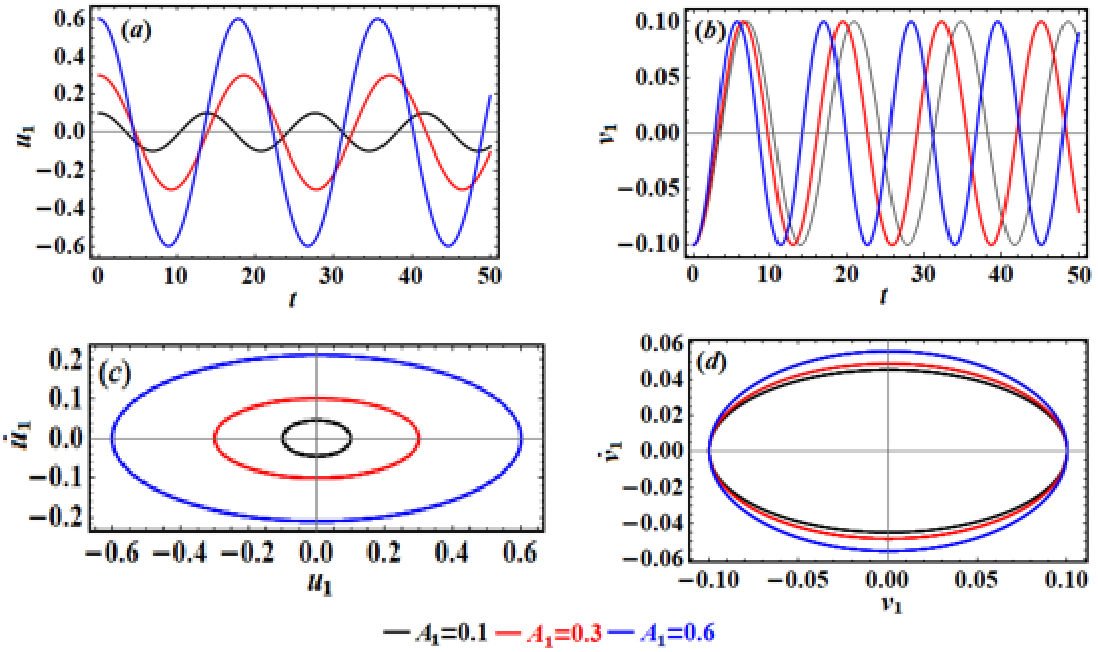

Fig. 12: Displays the behavior of the time-dependent solutions $u_1(t)$ and $v_1(t)$ for the system (35) and the plots of phase plane when the NPA is applied at $A_1(=0.1, 0.3, 0.6)$.

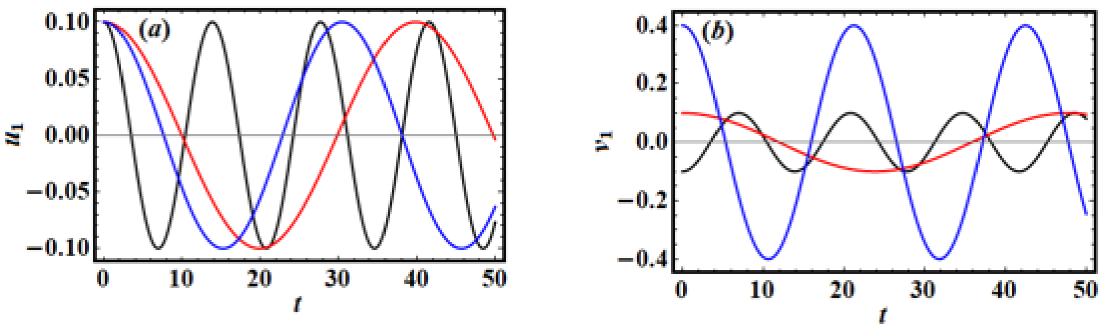

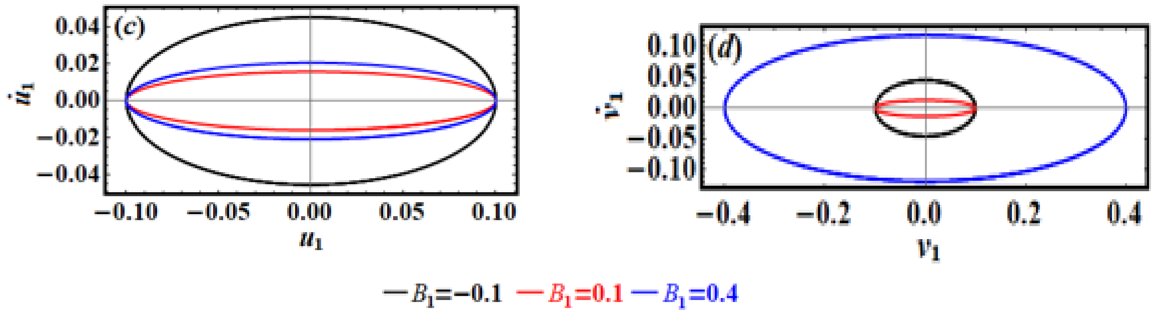

Fig. 13: Shows the time-dependent variation of u_1 and v_1 for the system (35) and the plots of phase plane when the NPA is applied at $B_1(=-0.1, 0.1, 0.4)$.

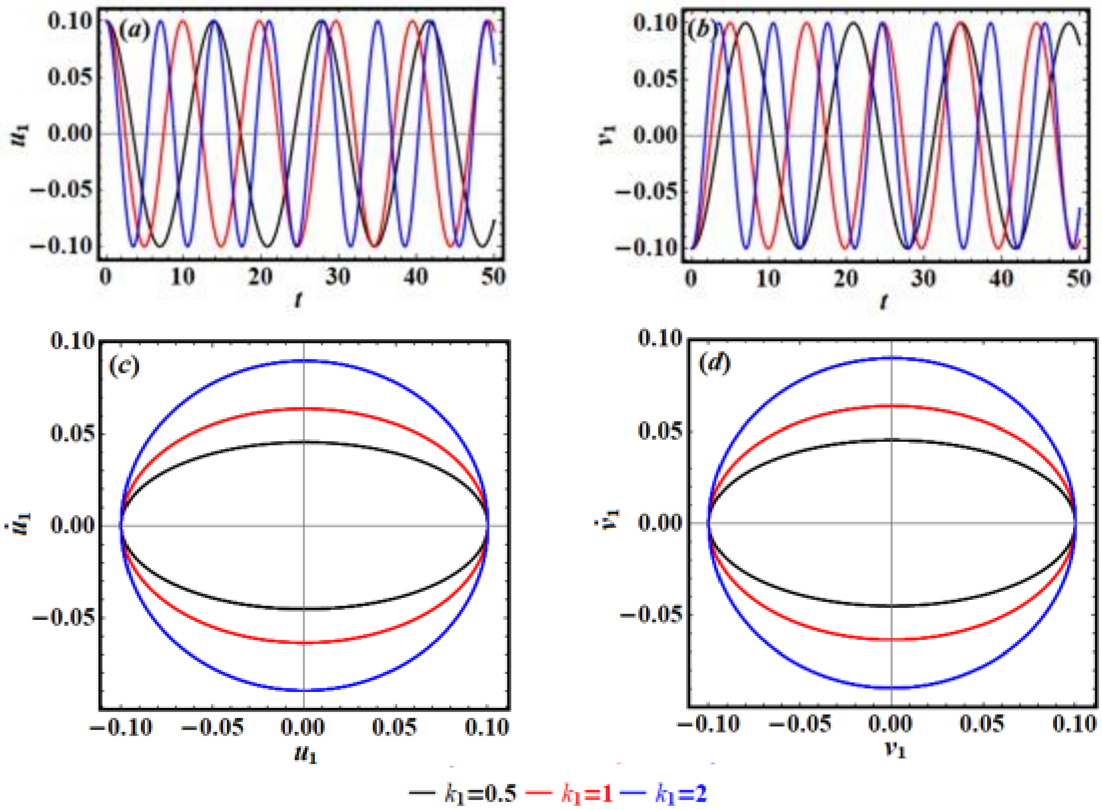

Fig. 14: Displays the change in the solutions $u_1(t)$ and $v_1(t)$ for the system (35) and the plots of phase plane when the NPA is applied at $k_1(=0.5, 1, 2)$.

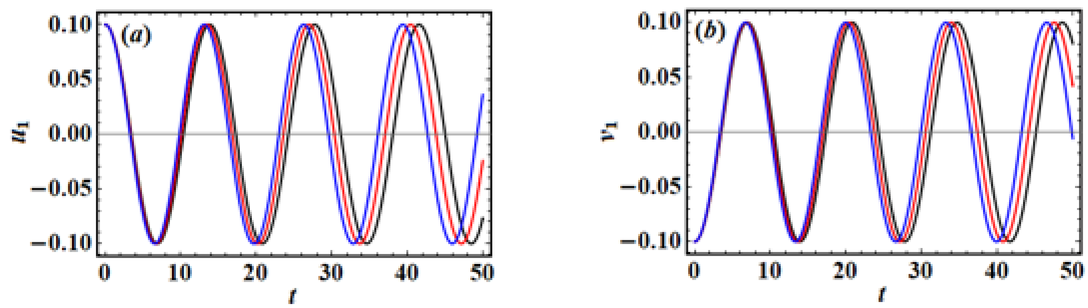

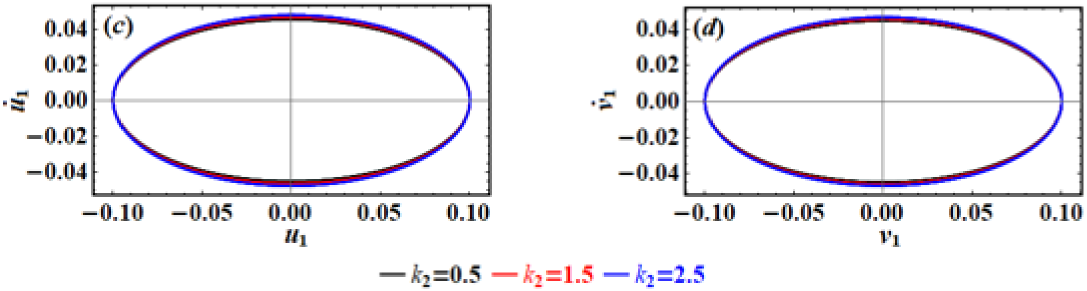

Fig. 15: Displays the variation of the solutions $u_1(t)$ and $v_1(t)$ for the system (35) and their phase plane plots when the NPA is applied at $k_2(=0.5, 1.5, 2.5)$.

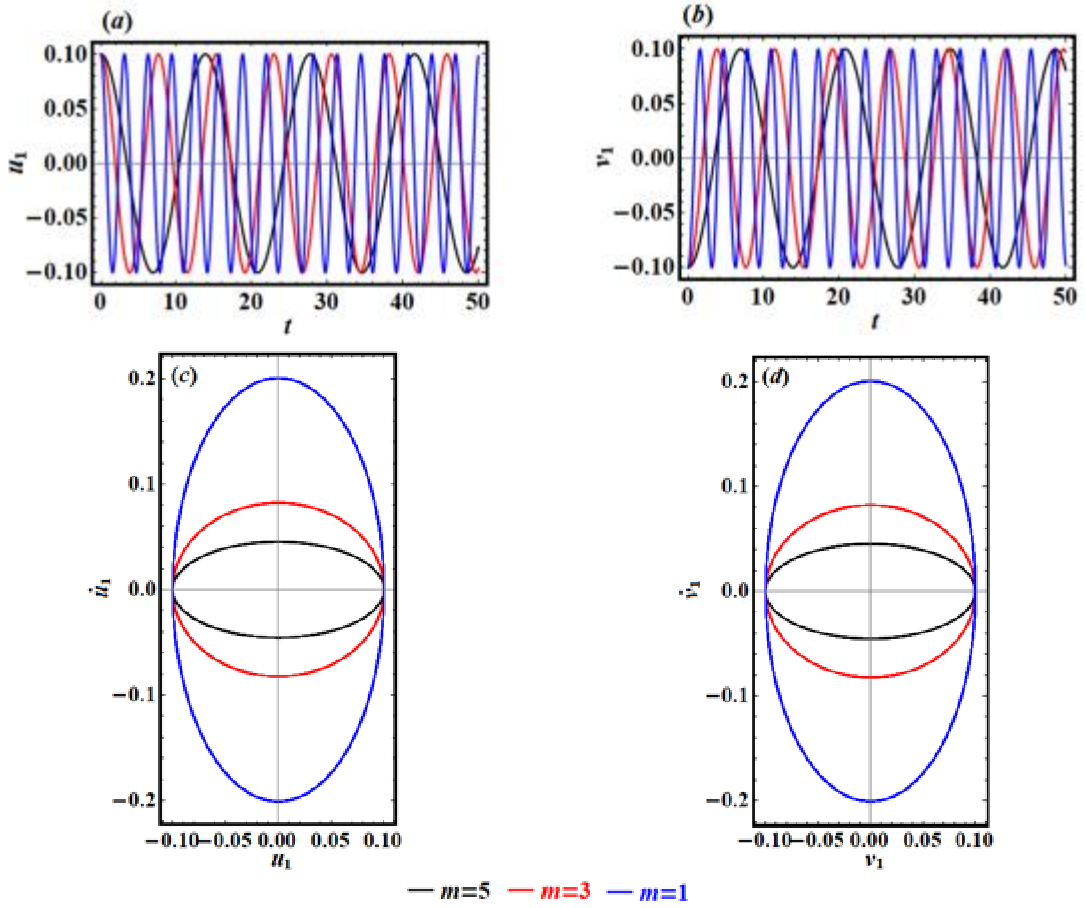

Fig. 16: Displays the plotted curves of the functions $u_1(t)$ and $v_1(t)$ for the system (35) and their phase plane plots when the NPA is applied at $m(=1,3,5)$.

3.3 *Example (3): Damped Coupled Harmonic Oscillator Fixed at the Two Ends*

A damped coupled harmonic oscillator fixed at two ends is made up of many masses joined together by springs, with the end masses fastened to stationary supports. This configuration adds more complexity than the free-end situation and is typical in mechanical systems when the ICs are fixed. Damped coupled harmonic oscillators fixed at both ends are used to model various physical systems, such as:

- **Electrical Circuits:** Resonant circuits with coupled inductors and capacitors.
- **Mechanical Systems:** Vibrations in buildings, bridges, and mechanical connections.
- **Biological Systems:** Coupled oscillations in biological tissues or organs.

Here, let us consider a two-equal masses system model fixed at the two ends as shown in Fig. 17, where X and

Y signify the directions of motion of the two masses. Furthermore, $m_1, b_1, k_3,$ and k_4 represent the mass of the two bodies, the damped coefficient, and the spring constants, respectively in the current example.

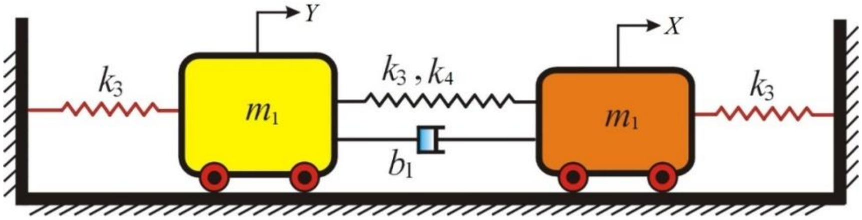

Fig. 17: Displays two masses connected by linear and nonlinear damped stiffness and fixed at the two ends.

The EOM of a damped coupled harmonic oscillator which is fixed from its ends are[2]:

$$\begin{cases} m_1\ddot{X} = -b_1(\dot{X} - \dot{Y}) - k_3 X - k_3(X - Y) - k_4(X - Y)^3 \\ m_1\ddot{Y} = -b_1(\dot{Y} - \dot{X}) - k_3 Y - k_3(Y - X) - k_4(Y - X)^3 \end{cases} \tag{41}$$

Eqs. (41) could be written as:

$$\begin{cases} \ddot{X} = -\dfrac{b_1}{m_1}(\dot{X} - \dot{Y}) - \dfrac{k_3}{m_1}(2X - Y) - \dfrac{k_4}{m_1}(X - Y)^3 \\ \ddot{Y} = -\dfrac{b_1}{m_1}(\dot{Y} - \dot{X}) - \dfrac{k_3}{m_1}(2Y - X) - \dfrac{k_4}{m_1}(Y - X)^3 \end{cases} \tag{42}$$

where m_1 is the mass of the two bodies, b_1 is the damped coefficient, k_1 and k_2 are the spring constants.

Again the suggested ICs of Eqs. (42) are usually considered as:

$$X(0) = C, Y(0) = D, \dot{X}(0) = 0, \text{and}\, \dot{Y}(0) = 0\,. \tag{43}$$

Eqs. (42) could be re-written as:

$$\begin{cases} \ddot{X} + F_5(\dot{Y}, \dot{X}) + F_6(X, Y) = 0 \\ \ddot{Y} + F_7(\dot{Y}, \dot{X}) + F_8(X, Y) = 0 \end{cases} \tag{44}$$

where

$$\begin{cases} F_5(\dot{Y}, \dot{X}) = \dfrac{b}{m}(\dot{X} - \dot{Y}) \\ F_6(X, Y) = \dfrac{k_1}{m}(2X - Y) + \dfrac{k_2}{m}(X - Y)^3 \\ F_7(\dot{Y}, \dot{X}) = \dfrac{b}{m}(\dot{Y} - \dot{X}) \\ F_8(X, Y) = \dfrac{k_1}{m}(2Y - X) + \dfrac{k_2}{m}(Y - X)^3 \end{cases}. \tag{45}$$

The trial solutions of the system (42) are assumed as:

$$w = C\cos\Omega_3 t, \text{ and } h = D\cos\Omega_4 t\,, \tag{46}$$

where C and D represent the amplitudes of the equivalent solutions A and B, whereas Ω_3 and Ω_4 are the total frequencies to be determined later.

The functions w and h satisfy the equivalent system:

$$\left.\begin{aligned} \ddot{w} + \mu_3\dot{w} + \omega_3^2 w = 0 \\ \ddot{h} + \mu_4\dot{h} + \omega_4^2 h = 0 \end{aligned}\right\}. \tag{47}$$

i. The Equivalent Frequencies:

The equivalent frequency can be calculated using the HFF by using the odd terms $F_6(X, Y)$ and $F_8(X, Y)$ as:

$$\omega_3^2 = \int_0^{2\pi/\Omega_3} wF_6(w,h)\,dt \Big/ \int_0^{2\pi/\Omega_3} w^2 dt\,, \tag{48}$$

$$\omega_4^2 = \int_0^{2\pi/\Omega_4} hF_8(w,h)\,dt \Big/ \int_0^{2\pi/\Omega_4} h^2 dt\,. \tag{49}$$

ii. The Equivalent Damping:

The equivalent damping term can be calculated utilizing the odd secular terms $F_5(X,Y)$ and $F_7(X,Y)$ by using the HFF as:

$$\mu_3 = \int_0^{2\pi/\Omega_3} \dot{w}\, F_5(\dot{w},\dot{h})dt \Big/ \int_0^{2\pi/\Omega_3} \dot{w}^2 dt\,. \tag{50}$$

$$\mu_4 = \int_0^{2\pi/\Omega_4} \dot{h}\, F_7(\dot{w},\dot{h})dt \Big/ \int_0^{2\pi/\Omega_4} \dot{h}^2 dt\,. \tag{51}$$

Now, it should be stated that the equivalent frequencies ω_3 and ω_4 as well as the equivalent damping coefficients μ_3 and μ_4 are evaluated via the MS and due to their long formulae, these forms are defined through the Appendix.

Assume the following standard normal forms:

$$\begin{cases} w(t) = W(t)Exp(-\mu_3 t/2), \\ h(t) = H(t)Exp(-\mu_4 t/2). \end{cases} \tag{52}$$

Consequently, substituting by Eqs. (52) into Eqs. (47), one gets:

$$\ddot{W}(t) + \Omega_3^2 W(t) = 0\,, \tag{53}$$

and

$$\ddot{H}(t) + \Omega_4^2 H(t) = 0\,, \tag{54}$$

where

$$\Omega_3^2 = \omega_3^2 - \mu_3^2/4\,, \tag{55}$$

$$\Omega_4^2 = \omega_4^2 - \mu_4^2/4\,. \tag{56}$$

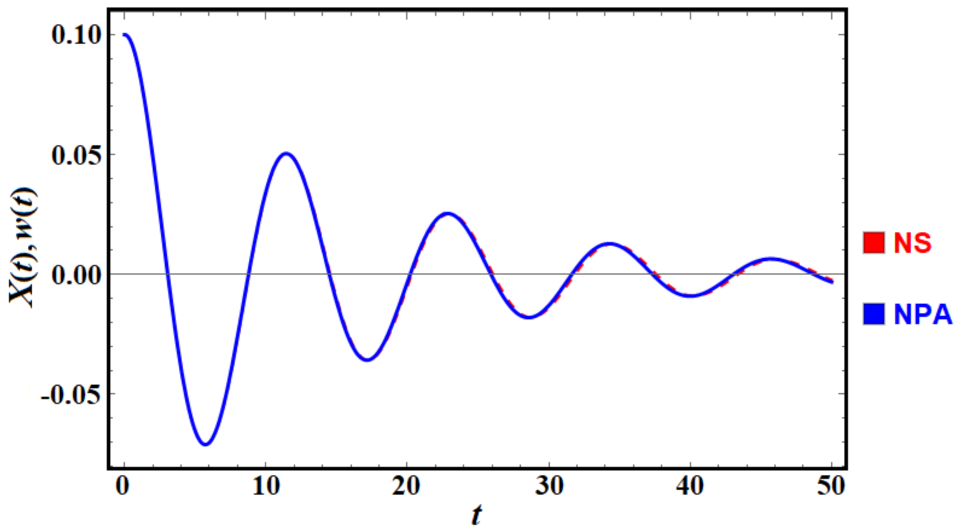

Fig. 18: Displays the matching between the two solutions of the non-linear dynamical system (42) and the NPA linear system (47) for the X oscillator.

It is important to note that the nonlinear ODEs specified in Eqs. (37) are represented by alternating linear equations in Eqs. (42). For comparing these systems, the MS is employed together with the *(NDSolve)* command; an example of the contained factors is illustrated below.

$$k_3 = 0.5, k_4 = 0.5, b_1 = 0.3, m_1 = 5, A_1 = 0.1, \text{ and } B_1 = -0.1$$

Figs. 18 and 19 are presented to show the solutions of the primary system (42) and the results of the equivalent system described in Eq. (47). The solid blue curve represents the solution of the original system (42), while the dotted red curve illustrates the NPA solution of the ODEs specified in Eq. (47). These figures are used to compare the two solutions over up to 50-time. It is found that the two curves are approximately congruent. Infinitesimal absolute errors between the original and the NPA solutions are attained, where the absolute error is 0.0019918 for the X - oscillator and equals 0.001341 for the Y - oscillator. Such convergence is attained also through Tables 3 and 4.

Table 3: Confirms the convergence of the real and NPA solutions for the X oscillator.

t	Real X oscillator	Approximate oscillator	Absolute error
0	0.1	0.1	0.
5	-0.0652812	-0.0653662	0.0000850652
10	0.0337988	0.0345977	0.000798902
15	-0.00991056	-0.0114844	0.00157382
20	-0.00520232	-0.00326987	0.00193245
25	0.0125261	0.0107818	0.00174437
30	-0.0141185	-0.0129668	0.00115167
35	0.0122398	0.0118345	0.000405243
40	-0.00881761	-0.00908469	0.000267082
45	0.00521551	0.00594133	0.000725823
50	-0.00221849	-0.00314719	0.000928701

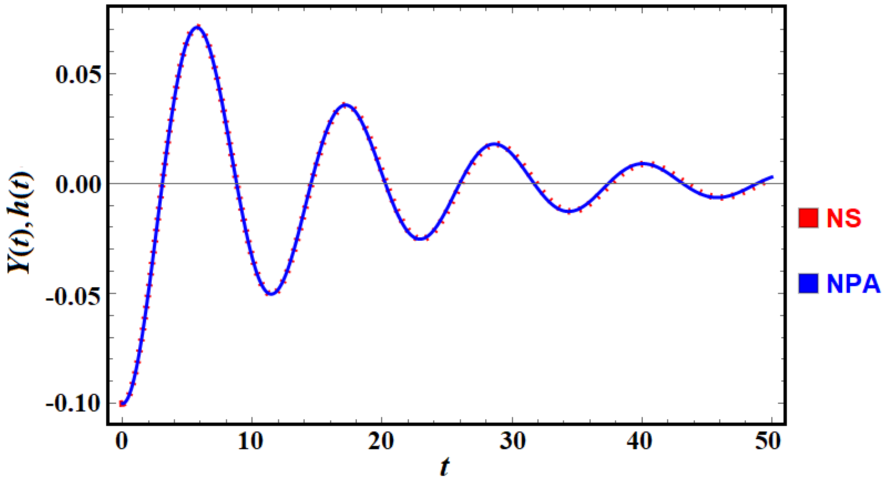

Fig. 19: Depicts the matching between the two solutions of the non-linear dynamical system (42) and the NPA linear system (47) for the Y -oscillator.

The strong concordance between the two curves, derived from a linear ODE and a nonlinear one, respectively, indicates that the nonlinear effects in the system are either minimal or exhibit behavior that closely resembles linearity under specific conditions. This may happen when the nonlinear variables exert limited influence on the overall system dynamics or when the system functions in a regime where the nonlinearities effectively "average out" or become linearized. In such instances, the solutions of the nonlinear system may closely mirror those of the linear system, resulting in practically indistinguishable curves. This phenomenon frequently arises in instances of weak nonlinearity, minor disturbances, or in conditions close to equilibrium points.

Table 4: Confirms the convergence of the real and NPA solutions for the Y oscillator.

t	Real Y -oscillator	Approximate oscillator	**Absolute error**
0	-0.1	-0.1	0.
5	0.0652812	0.0651253	0.000155861

10	-0.0337988	-0.034057	0.000258168
15	0.00991056	0.0107704	0.000859879
20	0.00520232	0.00397935	0.00122297
25	-0.0125261	-0.0113425	0.00118363
30	0.0141185	0.0133037	0.000814776
35	-0.0122398	-0.0119417	0.000298029
40	0.00881761	0.00900613	0.000188525
45	-0.00521551	-0.0057451	0.000529596
50	0.00221849	0.00290311	0.000684624

The graphical representations in Figs. 20-26 display the solutions of the system of Eqs. (47) obtained via the NPA for several parameter configurations, i.e. when $C(=0.1,0.5,0.9)$, $b_1(=0.3,0.8,1.3)$, $k_3(=0.5,1,2)$, $k_4(=0.5,1.5,2.5)$, and $m_1(=0.5,2.5,5)$. It must be highlighted that portions (*a*) and (*b*) show the time-dependent solutions w and h for the system of Eqs. (47), whereas parts (*c*) and (*d*) present the related phase plane plots. By closely examining the time history curves in parts (*a*) and (*b*), it becomes evident that these curves decay over time, which is anticipated due to the damping terms in the system. Furthermore, the rate of decay of the plotted curves changes depending on the influencing parameter, as observed in parts (*a*) and (*b*). The decay rate is more rapid for the curves in part (*b*) than those in part (*a*). Meanwhile, the phase plane curves in parts (*c*) and (*d*) exhibit spiral forms that converge to a fixed point and these forms differ based on the influencing parameters.

Decaying curves refer to the phenomenon where the amplitude of oscillations or the values of variables in the system decreases over time. This usually indicates the presence of damping terms $\mu_3\dot{w}$ and $\mu_4\dot{h}$ in the system (47), which gradually dissipate the system's energy, causing a reduction in amplitude. These curves often indicate that the system is stable and will eventually reach a steady state or equilibrium position. Analysis of the phase plane plots in portions (*c*) and (*d*) shows that decaying trajectories typically spiral inward towards a fixed point, suggesting the system is moving towards a stable equilibrium.

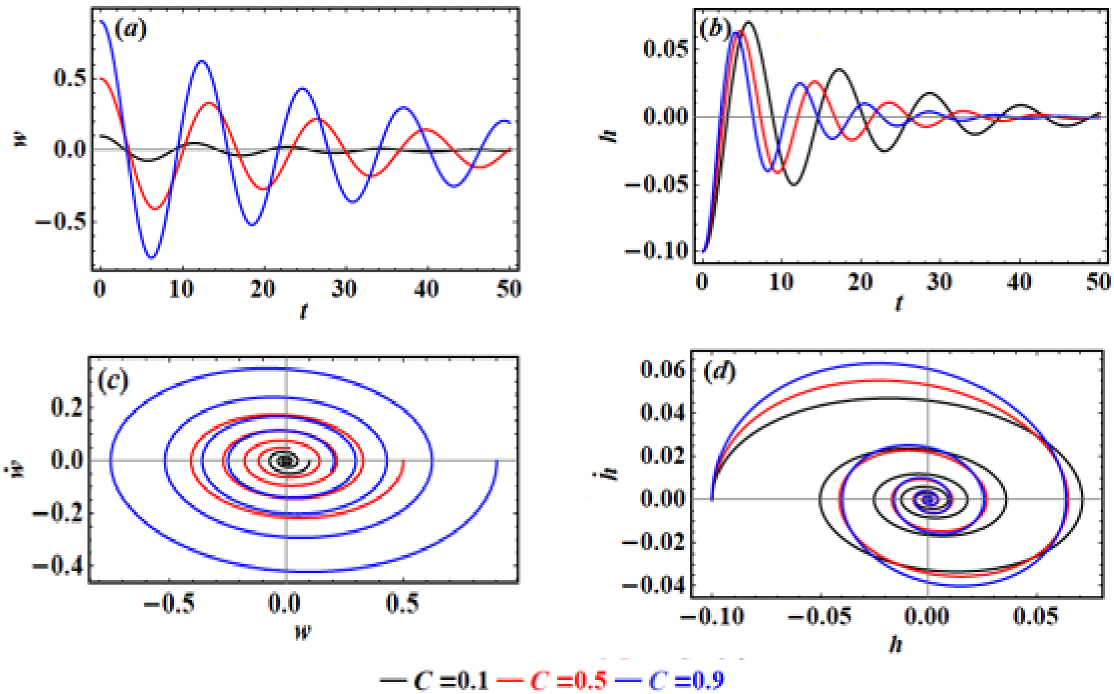

Fig. 20: Depicts the variation of the achieved solutions of system (47) using the NPA and their phase plane plots at $C(=0.1,0.5,0.9)$.

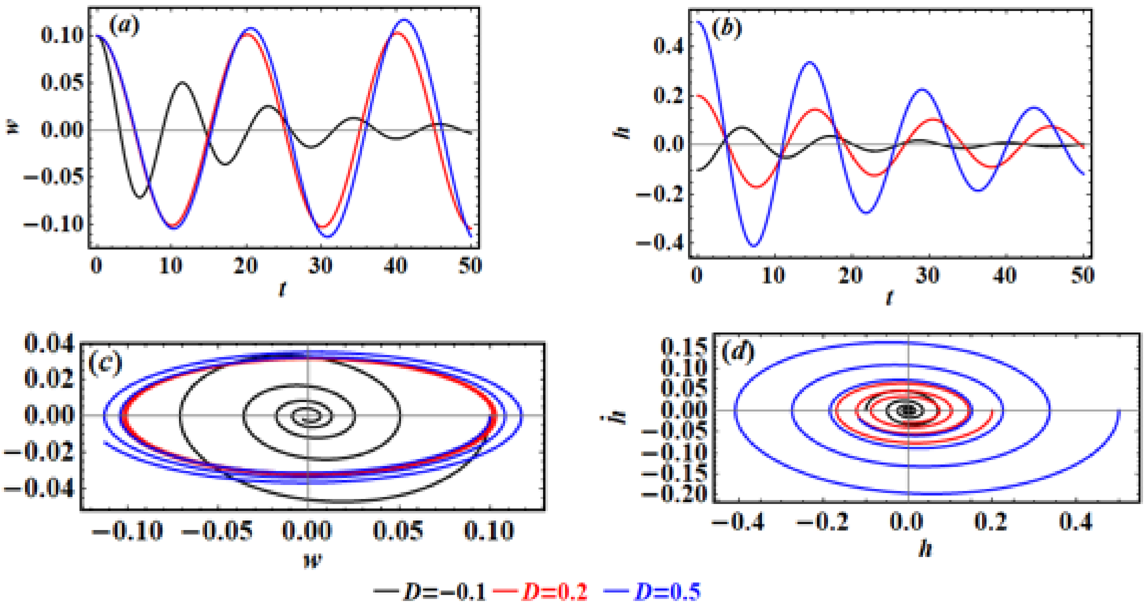

Fig. 21: Depicts the variation of the achieved solutions of system (47) using the NPA and their phase plane plots at $D(=-0.1, 0.2, 0.5)$.

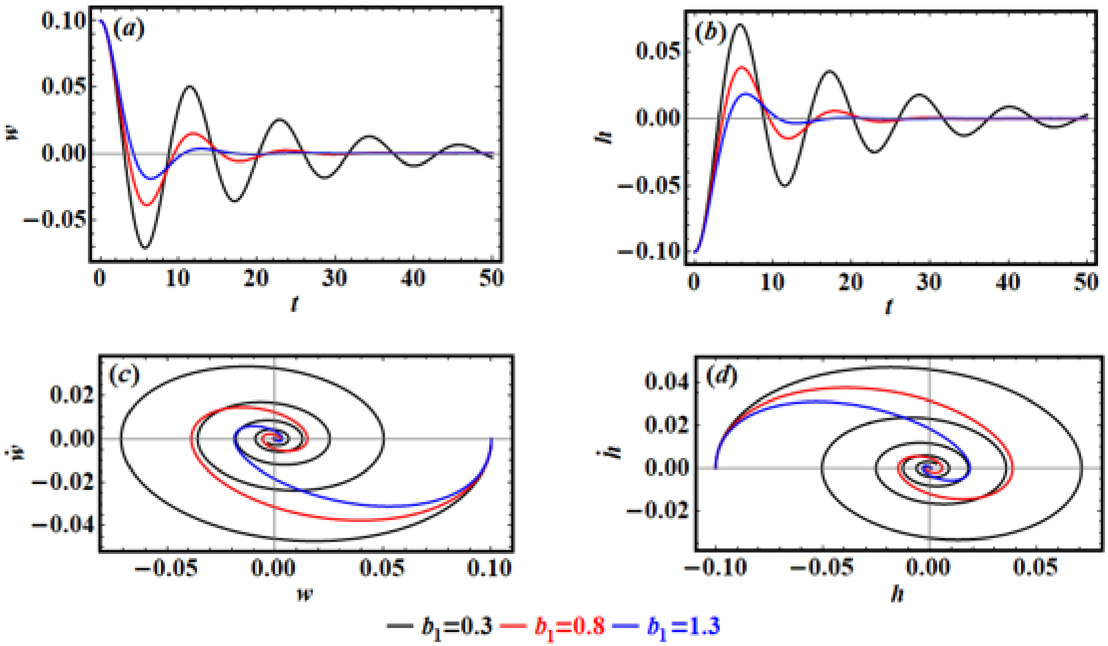

Fig. 22: The observed change for the solutions of system (47) according to the NPA and their phase plane plots at $b_1(=0.3, 0.8, 1.3)$.

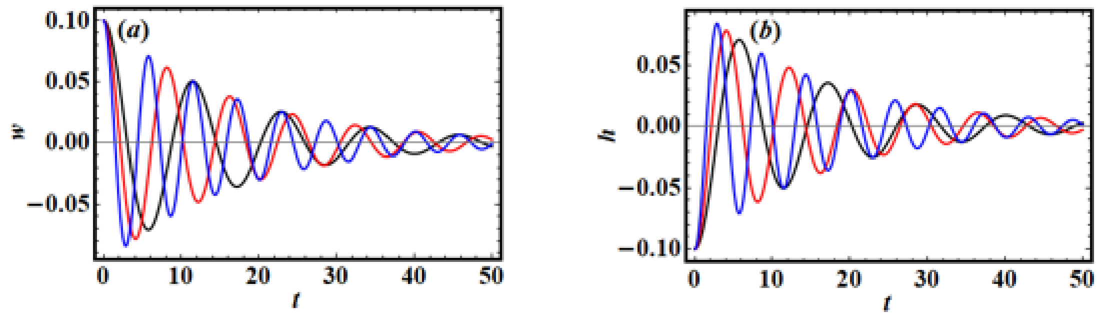

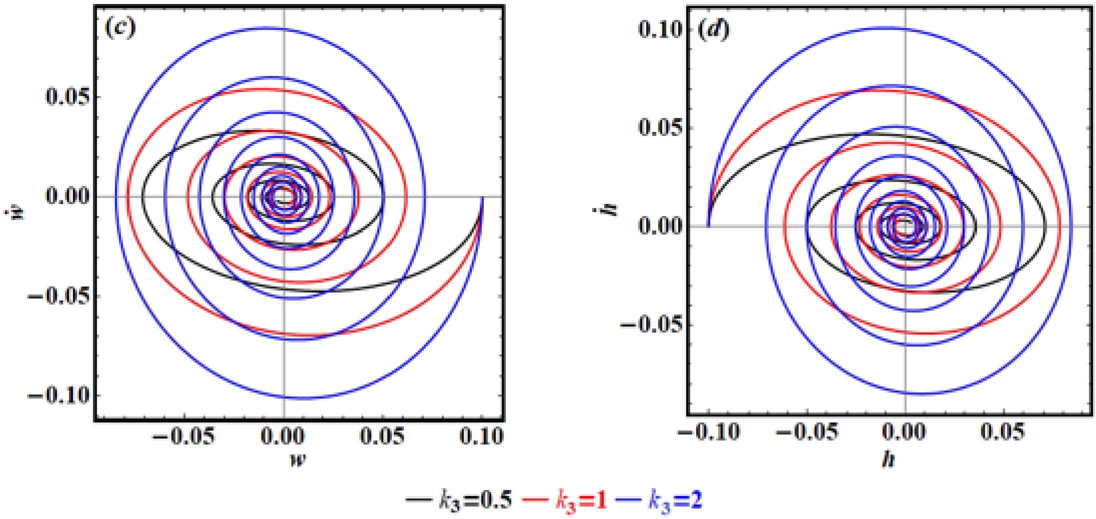

Fig. 23: The time-variation of the functions w and h, and their projections in the planes $w\dot{w}$ and $h\dot{h}$ at $k_3(=0.5,1,2)$.

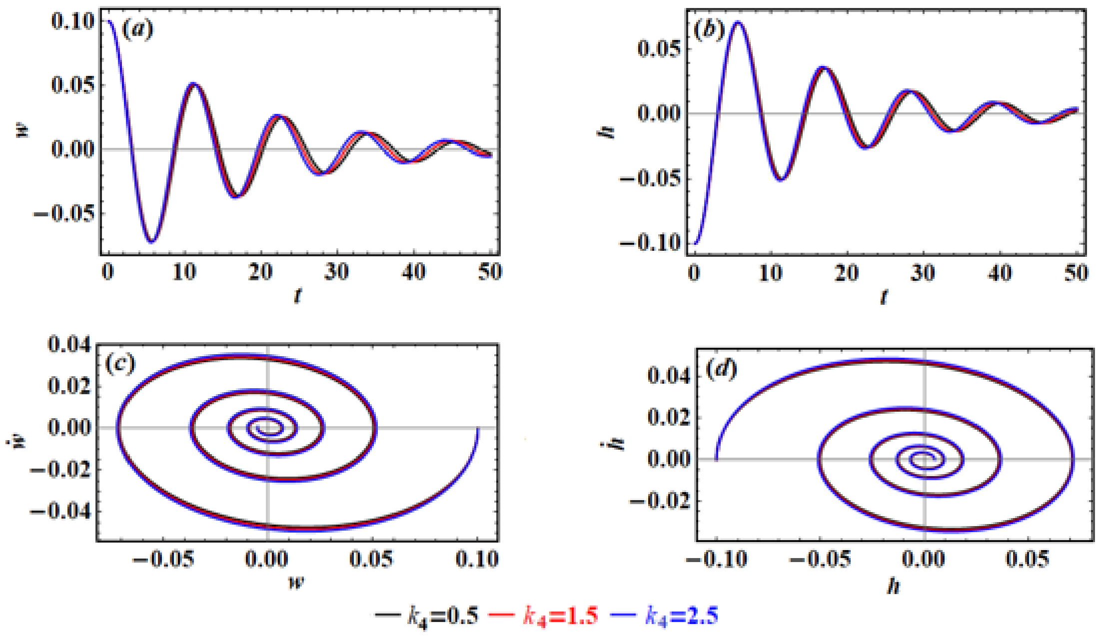

Fig. 24: The sketches of $w(t)$ and $h(t)$, and their projections in the planes $w\dot{w}$ and $h\dot{h}$ at $k_4(=0.5,1.5,2.5)$.

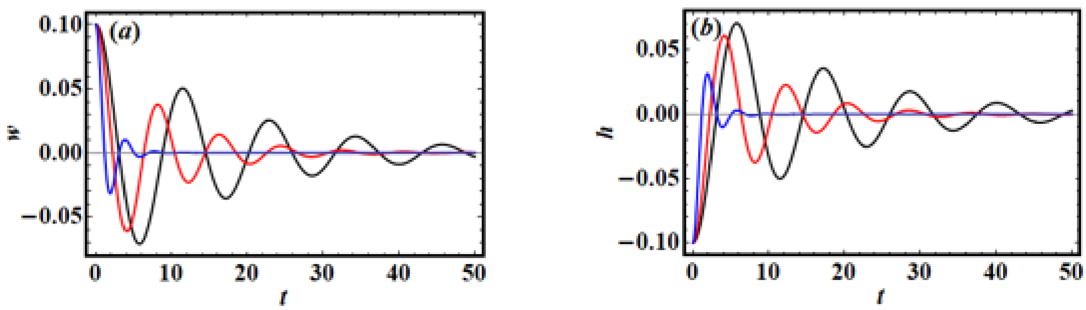

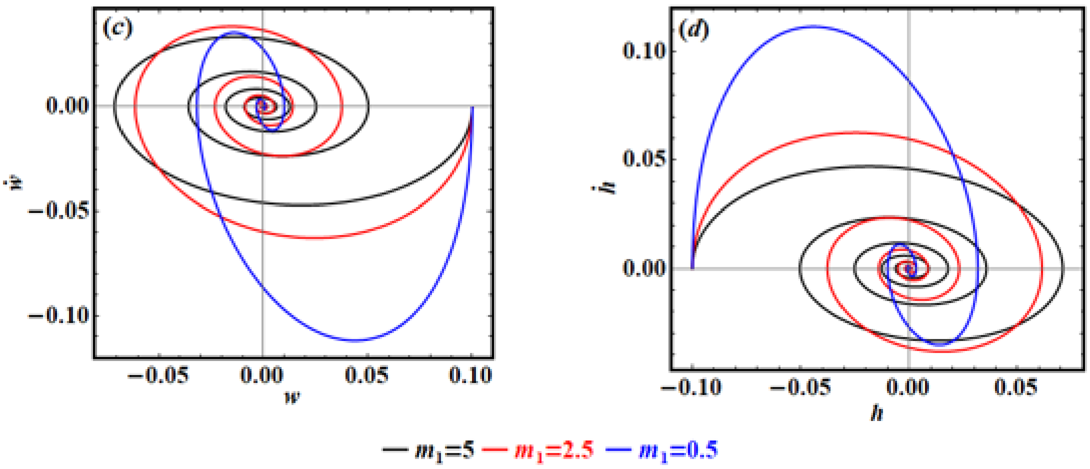

Fig. 25: The time-behaviors of w and h, and their related phase plane plots at $m_1(=0.5, 2.5, 5)$.

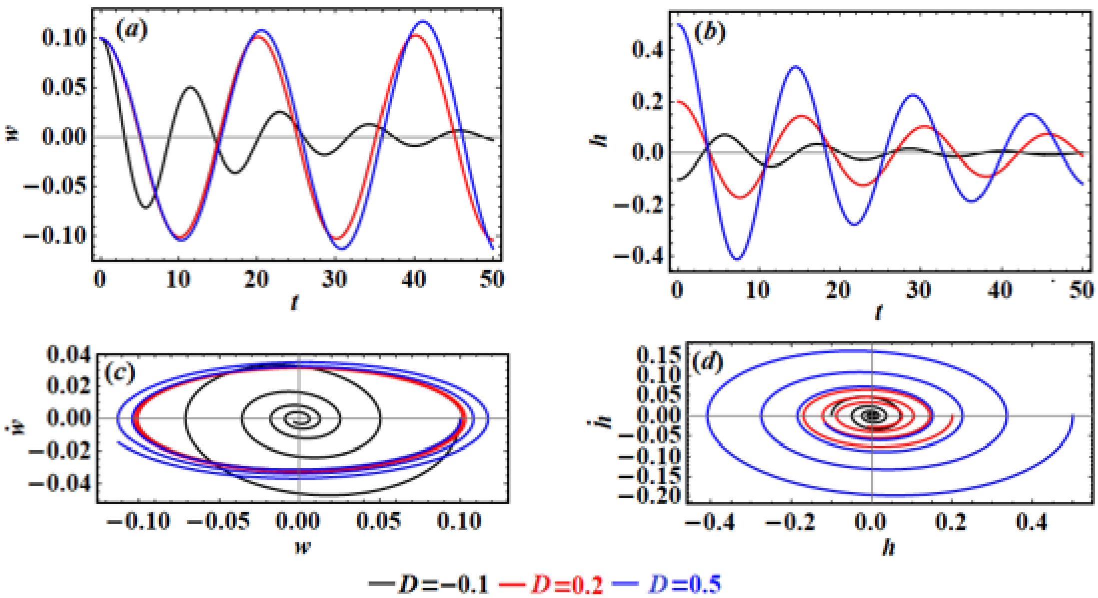

Fig. 26: The behavior of $w(t)$ and $h(t)$, and the related phase plane curves at $D(=-0.1, 0.2, 0.5)$.

3.4 Example (4): Non-Damped Coupled Harmonic Oscillator Fixed at the Two Ends

Inspecting the conservative state of the coupled system as given in Eqs. (42), when the damping forces' influences vanish ($b_1 = 0$). The coupled harmonic oscillator (42) without damping can be expressed as follows [2]:

$$\begin{cases} \ddot{X} = -\dfrac{k_3}{m_1}(2X - Y) - \dfrac{k_4}{m_1}(X - Y)^3 \\ \ddot{Y} = -\dfrac{k_3}{m_1}(2Y - X) - \dfrac{k_4}{m_1}(Y - X)^3. \end{cases} \tag{57}$$

Eqs. (52) might be re-written as:

$$\begin{cases} \ddot{X} + F_6(X, Y) = 0 \\ \ddot{Y} + F_8(X, Y) = 0 \end{cases}, \tag{58}$$

where $F_6(X, Y)$ and $F_8(X, Y)$ are the same functions that were defined before through Eqs. (45)

The trial solutions of the system (57) are assumed, in the following form:

$$w_1 = C_1 \cos \delta_3 t, h_1 = D_1 \cos \delta_4 t\,, \tag{59}$$

where C_1 and D_1 represent the amplitudes of the equivalent solutions w_1 and h_1, while δ_3 and δ_4 are the total frequencies in this case and they will be determined later.

The functions w_1 and h_1 satisfy the equivalent system:

$$\begin{cases} \ddot{w}_1 + \delta_3^2 w_1 = 0 \\ \ddot{h}_1 + \delta_4^2 h_1 = 0 \end{cases} \tag{60}$$

where the equivalent frequencies can be calculated by means of the HFF and by using the odd terms $F_6(X,Y)$ and $F_8(X,Y)$ as:

$$\delta_3^2 = \int_0^{2\pi/\delta_3} w_1 F_6(w_1, h_1)\, dt \Big/ \int_0^{2\pi/\delta_3} w_1^2 dt\,. \tag{61}$$

$$\delta_4^2 = \int_0^{2\pi/\delta_4} h_1 F_8(w_1, h_1)\, dt \Big/ \int_0^{2\pi/\delta_4} h_1^2 dt\,. \tag{62}$$

These integrals are evaluated by MS and their values are equal to their correspondence ω_3 and ω_4 in the preceding case which are obtained in the Appendix.

Following the same previous procedure when b vanishes and by plotting the solutions of the nonlinear and the equivalent linear equations, a very convergence is found between the two solutions. Using the data $k_3 = 0.5, k_4 = 0.5, b_1 = 0, m_1 = 5, C_1 = 0.1,$ and $D_1 = -0.1$, it is found that the absolute error equals 0.000522 for the x oscillator and 0.00598 for the y oscillator, as graphed in Figs. 27 and 28, respectively.

The significant agreement between the two curves, originating from a linear ODE and a nonlinear one, respectively, suggests that the nonlinear effects in the system are either negligible or demonstrate behavior that nearly approximates linearity under certain conditions. This may occur when the nonlinear variables exert minimal influence on the overall system dynamics or when the system operates in a regime where the nonlinearities effectively "average out" or become linearized. In such cases, the solutions of the nonlinear system may strongly resemble those of the linear system, yielding virtually indistinguishable curves. This phenomenon often occurs in situations of modest nonlinearity, slight shocks, or near equilibrium points.

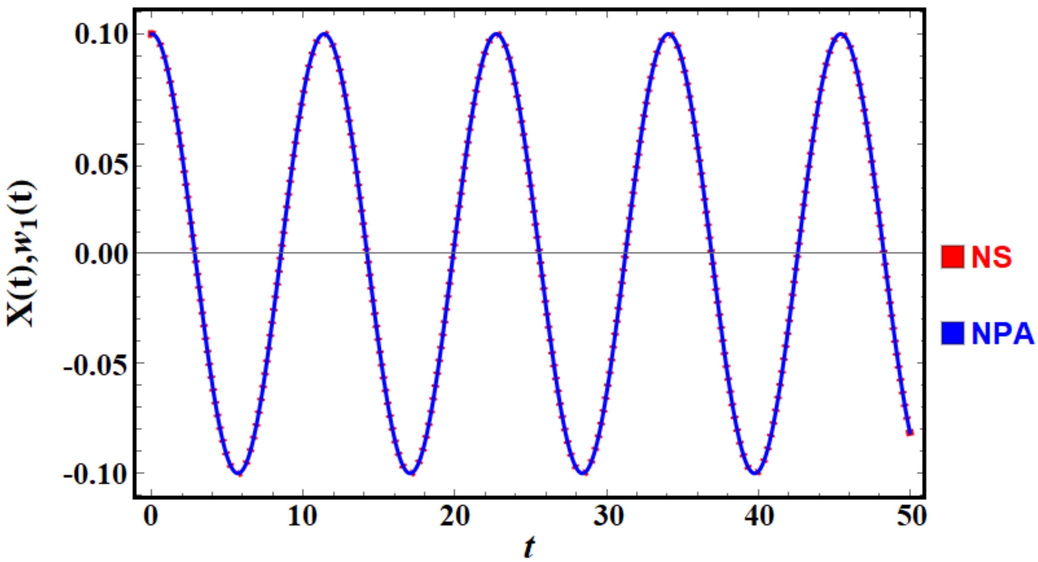

Fig. 27: Illustrates the matching between the two solutions of the non-damped dynamical system (57) and the NPA linear system for the X oscillator.

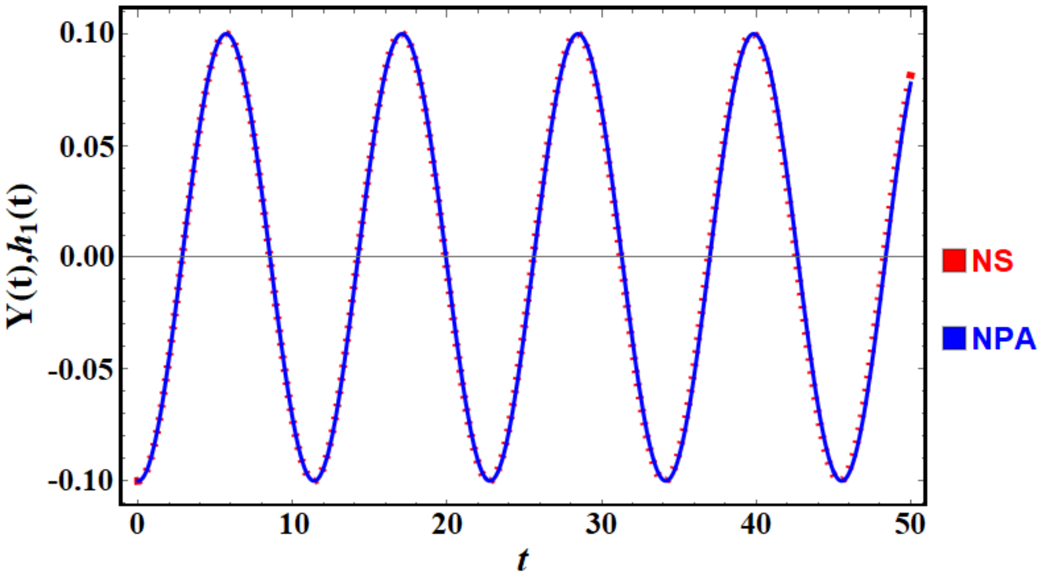

Fig. 28: Depicts the matching between the two solutions of the non-damped dynamical system (57) and the NPA linear system for the Y oscillator.

In light of the analysis in section 3.3, the obtained non-perturbative solutions of equations of system (57) can be easily derived. These solutions are displayed in Figs. 29, 30, 31, 32, 33, and 34 using the previously specified values for parameters $C_1 = D_1 (= 0.1, 0.5, 0.9)$, $b_1 (= 0.3, 0.8, 1.3)$, $k_3 (= 0.5, 1, 2)$, $k_4 (= 0.5, 1.5, 2.5)$, and $m_1 (= 0.5, 2.5, 5)$. The time-dependent behaviors of the solutions are illustrated in portions (*a*) and (*b*) of these figures, with the corresponding phase plane diagrams shown in parts (*c*) and (*d*). Inspection of the time history waves indicates that these waves exhibit periodic forms throughout the entire duration. The graphs indicate that the oscillation numbers for both solutions w_1 and h_1 change based on the parameters in effect. For the solution w_1, the wavelengths and amplitudes of the waves in Fig. 29*a* decrease as the amplitude's parameter C_1 increases. In contrast, the amplitudes of the waves for the solution h_1 remain constant, while the number of vibrations moderately increases with higher D_1 values, as shown in Fig. 29*b*. The related plots in the $w_1 \dot{w}_1$ and $h_1 \dot{h}_1$ planes show the relationship between the solutions and their first derivatives, excluding the time parameter. These plots display symmetric closed curves around their vertical or horizontal axes, offering insight into the stability or steady-state behaviors of the solutions, as depicted in Figs. 29*c* and 29*d*. It should be mentioned that when the trajectory follows a closed curve repeatedly, it indicates that the system returns to the same state after each period, demonstrating stability. The inspection of the plotted curves in Fig. 30 shows the time-dependent variations of the solutions w_1 and h_1 when $D_1 (= -0.1, 0.2, 0.5)$, as seen in parts (a) and (b). Periodic waves are produced with different amplitudes according to the values of D_1. Furthermore, symmetric closed curves that express the stability of w_1 and h_1 are presented in parts (c) and (d) for these solutions.

Figs. 31*a* and 31*b* depict how the time-dependent functions w_1 and h_1 change as the parameter k_3 varies. Despite constant amplitudes, the number of fluctuations increases with higher values of the same parameter, indicating a decrease in wavelength. These results are portrayed in Figs. 31*c* and 31d in the forms of symmetric closed curves, each featuring three closed curves that may represent one limit cycle per k_3 value, showing that the solutions are stable and free from chaotic behavior as k_3 changes. The time-dependent functions for the same solutions with the varying of k_4 are shown in Figs. 32*a* and 32*b*. The amplitudes and number of fluctuations remain constant with increasing k_4 values, indicating similar curve configurations. Figs. 32*c* and 32*d* present closed curves obtained by excluding time t from the solutions and their first derivatives.

The variation of functions w_1 and h_1 with mass variation $m_1 (= 0.5, 2.5, 5)$ is depicted in Figs. 33*a* and 33*b*. The data clearly demonstrate that changes in mass parameters significantly influence periodic wave behavior, with the number of oscillations decreasing as the mass increases. Therefore, as the mass mmm increases, the wavelengths of the plotted waves expand, while the amplitudes remain unchanged. The phase plane plots in Figs. 33*c* and 33*d*, which show three distinct closed curves for varying mass values, illustrate that the system's motion remains stable throughout the entire time interval.

The inspection of the curves displayed in Figs. 34 shows that the temporal histories of the solutions of system (57), i.e., for the absence of the damping parameters, when D_1 varies as seen in parts (*a*) and (*b*). The behaviors of the presented waves have periodic forms, in which the oscillation numbers increase with the increase of D_1 values while their amplitudes remain stationary, as in part (*a*). On the other hand, the oscillations number decreases with the increase in D_1 values, whereas their amplitudes increase. The related phase plane plots of these solutions are portrayed in portions (*c*) and (*d*), which have the forms of closed symmetric curves about the horizontal and vertical axes.

Based on this analysis, one can conclude that periodic solutions suggest that the system's behavior can be predicted over time. If a system demonstrates periodic behavior, future states can be anticipated based on its present state, which is useful for both theoretical studies and practical applications. Moreover, the closed symmetric curves observed in phase plane plots offer a valuable and clear depiction of the system's periodic behavior, stability, and energy characteristics, enhancing both theoretical and practical analysis.

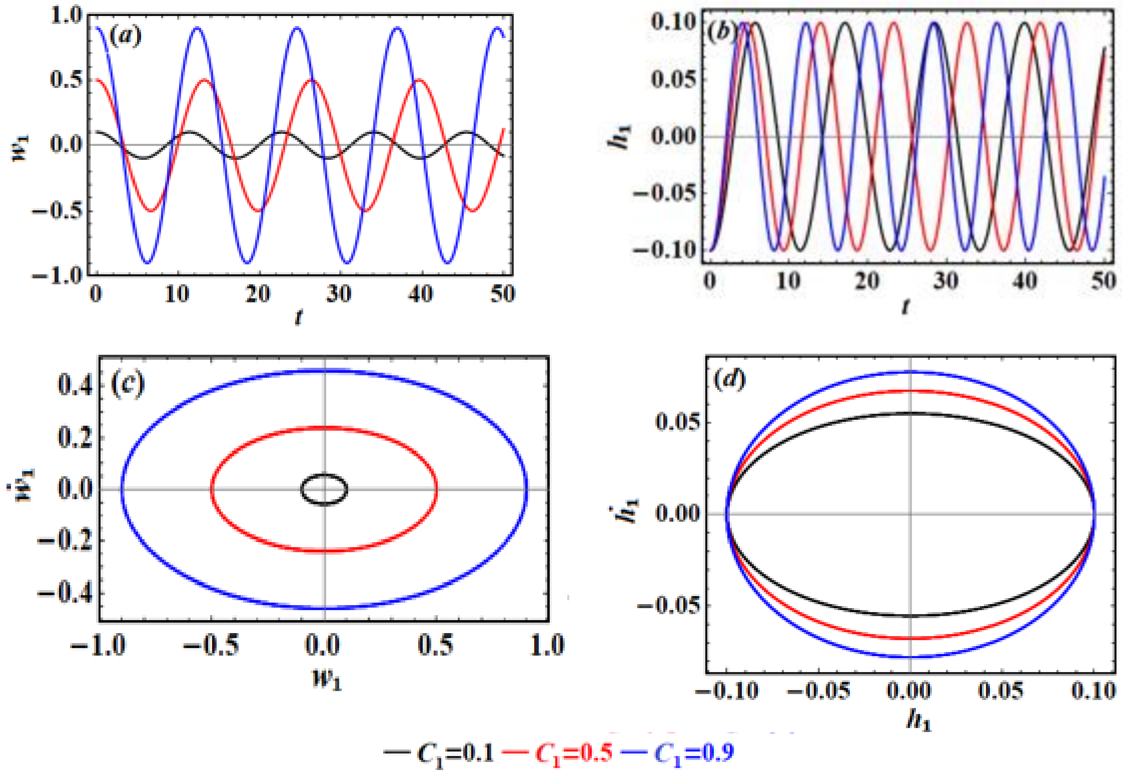

Fig. 29: Variation of the solutions of system (52) using the NPA and their phase plane plots at $b_1 = 0$ and $C_1 (= 0.1, 0.5, 0.9)$.

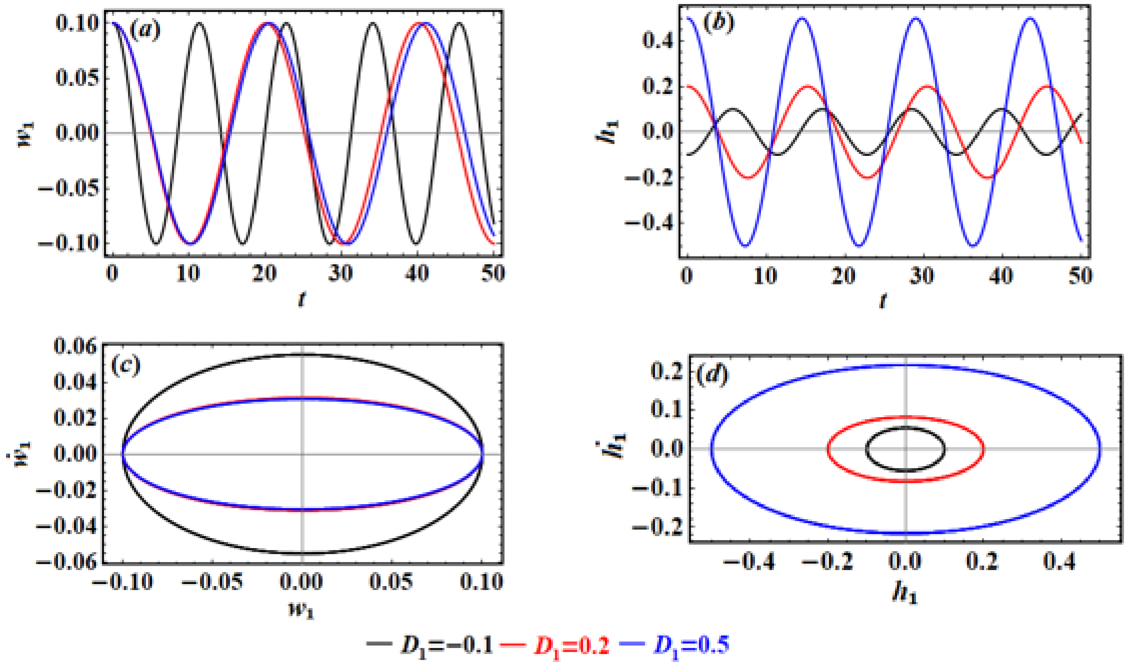

Fig. 30: Variation of the solutions of system (52) using the NPA and their phase plane plots at $b_1 = 0$ and $D_1 (= -0.1, 0.2, 0.5)$.

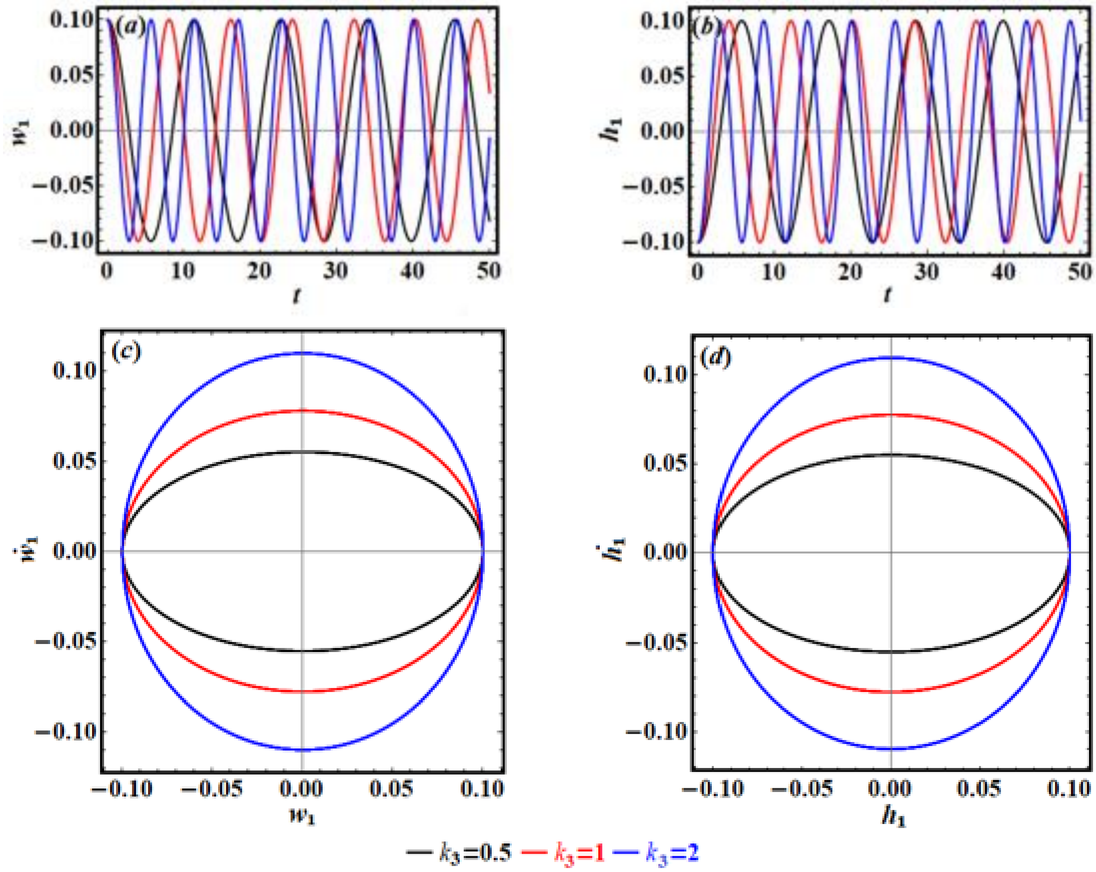

Fig. 31: The temporal behavior for the solutions of system (52) using the NPA and their phase plane plots at $b_1 = 0$ and $k_3 (= 0.5, 1, 2)$.

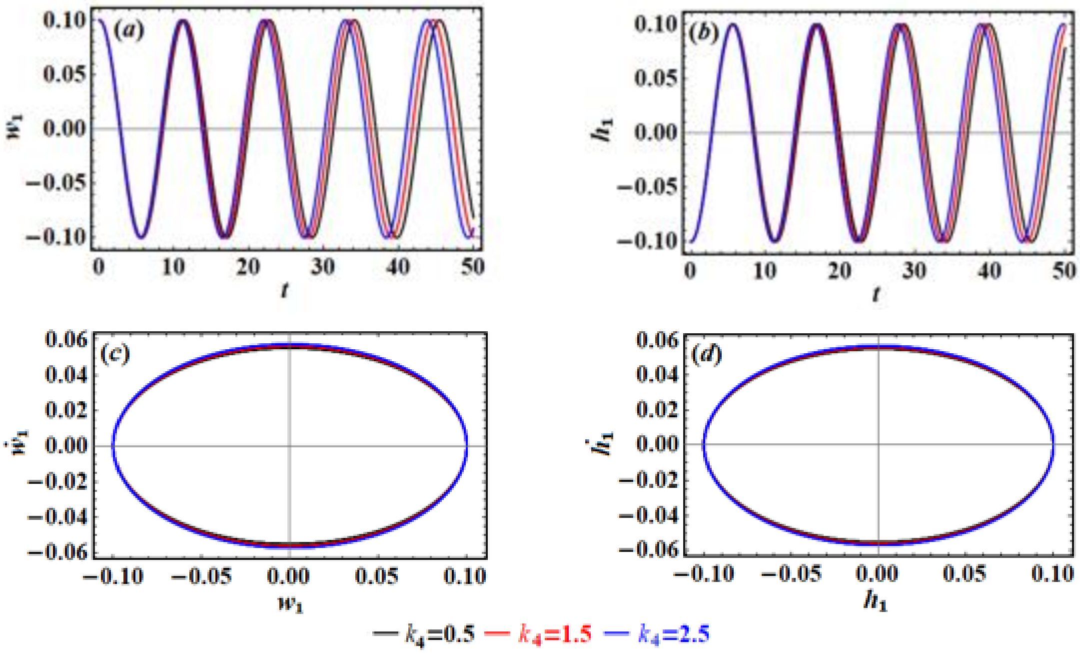

Fig. 32: The time history of the solutions of system (52) using the NPA and the related phase plane diagrams at $b_1 = 0$ and $k_4 (= 0.5, 1.5, 2.5)$.

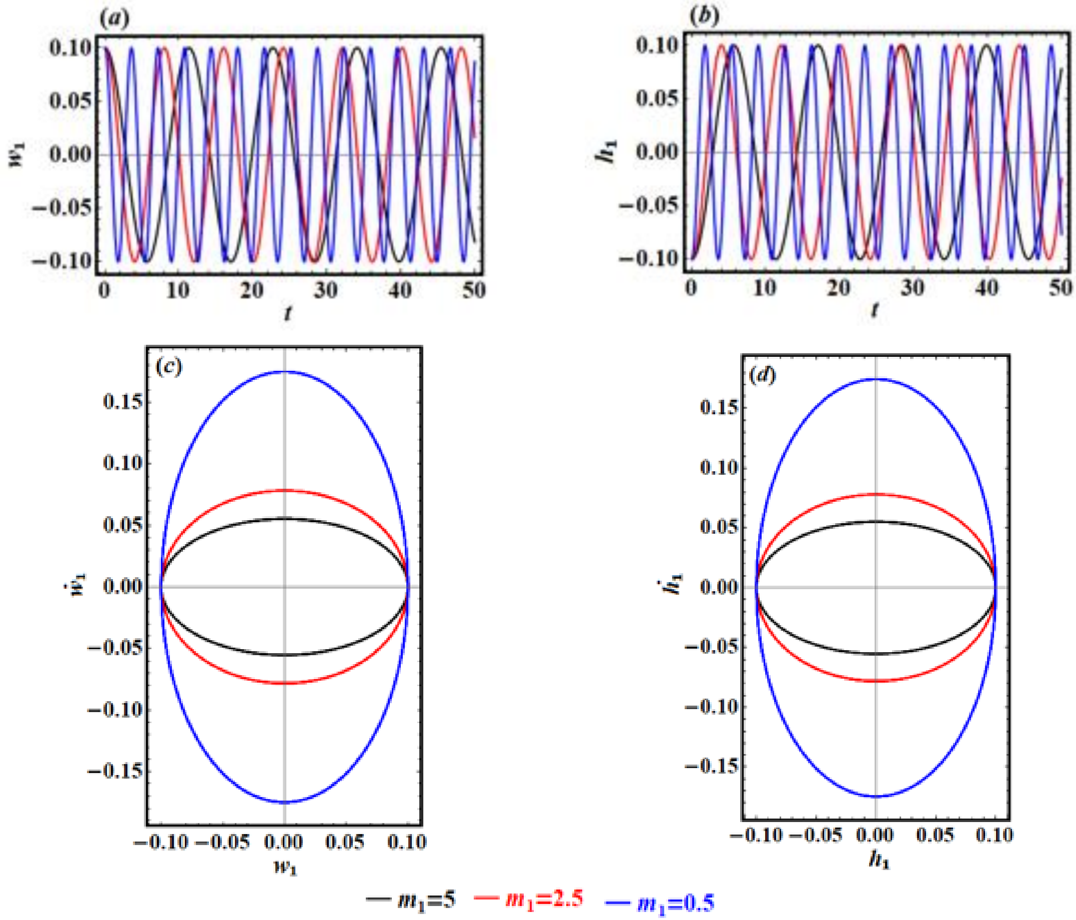

Fig. 33: The time-behaviors of w and h, and their related phase plane plots at $b_1 = 0$ and $m_1 (= 0.5, 2.5, 5)$.

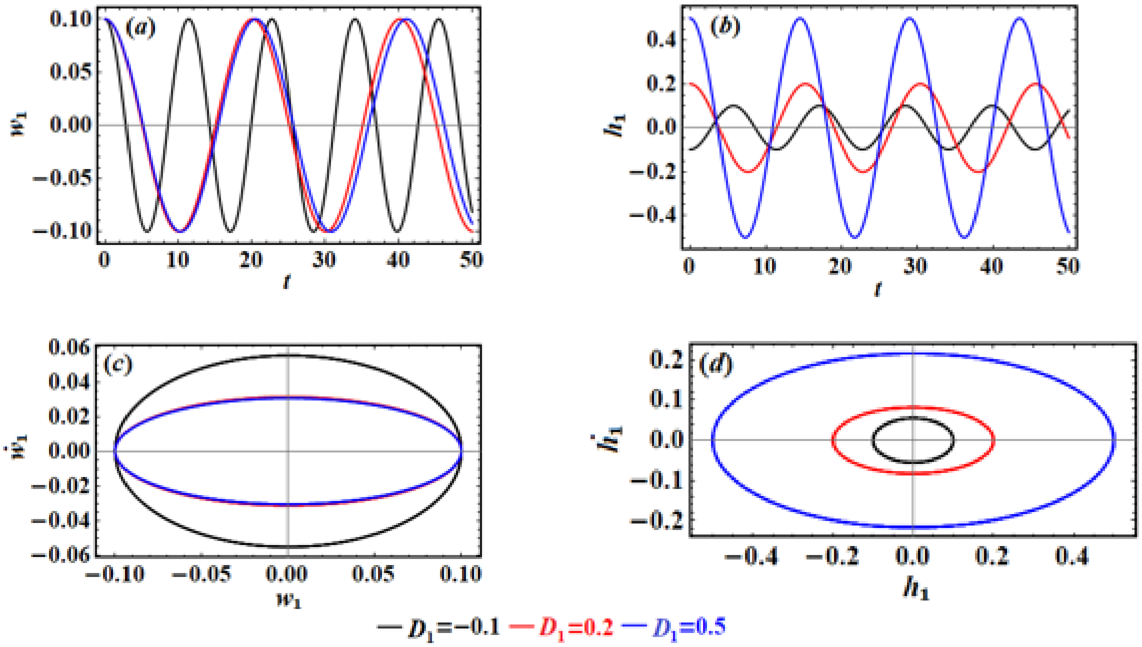

Fig. 34: The time history of the functions w_1 and h_1, and the related phase plane curves at $b_1 = 0$ and $D_1(=-0.1, 0.2, 0.5)$.

4. Conclusions

Concentrated coupled harmonic nonlinear oscillators are crucial of representing various physical systems, including electrical circuits, mechanical structures, and certain biological systems. The objective of this study was to analyze the honest NPA in order to obtain alternating periodic solutions for damped and conservative coupled mass-spring systems. These systems have both linear and nonlinear stiffness and demonstrate nonlinear free vibrations. The NPA mostly relies on the HFF. The proposed approach was presented through two practical examples of TDOF oscillation systems to showcase its accuracy, efficacy, and applicability. The objective of this study is to provide approximate solutions for small amplitude parametric components, without any constraints, by deviating from typical perturbation methods. In addition, the method was expanded to discover optimal solutions for the nonlinear coupled oscillators. The iterative calculations of the solutions to the parametric nonlinear fluctuation require a rapid estimation of the frequency-amplitude correlation. The obtained solutions for the examined models and two special cases are shown graphically. The keys of the present calculations may be summarized as follows:

- **i.** The parametric equation generated was verified using the MS, it demonstrates exceptional concurrence with the NS of the original system.
- **ii.** The graphs reveal the temporal behaviors of the models and the favorable impact of the applied parameters.
- **iii.** Consistent decay behavior in the time histories of these solutions implies stability.
- **iv.** Furthermore, the phase plane curves, displayed in multiple plots, exhibit inward spirals converging at a single point.
- **v.** Periodic behaviors were observed in limited cases as several parameters vary. Therefore, the phase plane curves took the form of symmetric closed loops, producing limit cycles with isolated closed curves.
- **vi.** The current methodology appears to be direct, appealing, promising, potent, and captivating. It can be used for several types of interconnected dynamical systems.

Appendix

The integrals (25) – (28) as evaluated by MS are given as:

$$\omega_1^2 = \frac{\omega_1}{8\pi A m}\left(a_1 \sin\left(\frac{2\pi\omega_2}{\omega_1}\right) + a_2 + a_3 \sin\left(\frac{4\pi\omega_2}{\omega_1}\right) + a_4 \sin\left(\frac{6\pi\omega_2}{\omega_1}\right)\right),$$

$$\omega_2^2 = \frac{1}{a_5}\left(a_6 \sin\left(\frac{2\pi\omega_1}{\omega_2}\right) + a_7 \sin\left(\frac{4\pi\omega_1}{\omega_2}\right)\right),$$

$$\mu_1 = a_8 \sin\left(\frac{2\pi\omega_2}{\omega_1}\right),\ \ \mu_2 = a_9 \sin\left(\frac{2\pi\omega_1}{\omega_2}\right),$$

where

$$a_1 = \omega_1\left(\frac{2B\omega_2\left(3\omega_1^2(28A^2k_2 + 9B^2k_2 + 12k_1) - \omega_2^2(3k_2(4A^2 + B^2) + 4k_1)\right)}{9\varpi_1^4 - 10\omega_1^2\omega_2^2 + \omega_2^4}\right),$$

$$a_2 = \frac{2\pi A(3k_2(4A^2 + B^2) + 4k_1)}{\omega_1},\ a_3 = 3B^2k_2\left(\frac{A(\omega_1^2 - 2\omega_2^2)}{\omega_1^2\omega_2 - \omega_2^2}\right),\ \ a_4 = 3B^2k_2\left(\frac{2B\omega_2}{\omega_1^2 - 9\omega_2^2}\right),$$

$$a_5 = 8\pi Bm\omega_1(\omega_1^4 - 10\omega_1^2\omega_2^2 + 9\omega_2^4),\ \ a_6 = -8A\omega_1^2\omega_2(k_1(\omega_1^2 - 9\omega_2^2) + 3B^2k_2(\omega_1^2 - 7\omega_2^2)),$$

$$a_7 = B(\omega_1^2 - 9\omega_2^2)(4(2k_1 + 3A^2k_2)\pi\omega_1(\omega_1^2 - \omega_2^2) - 3A^2k_2\omega_2(-2\omega_1^2 + \omega_2^2)),$$

$$a_8 = \frac{b}{m}\left(1 + \frac{B\omega_1\omega_2}{A\pi(\omega_1^2 - \omega_2^2)}\right),\ \ a_9 = \frac{b}{m}\left(1 - \frac{A\omega_1\omega_2}{B\pi(\omega_1^2 - \omega_2^2)}\right).$$

The integrals (48) – (51) as evaluated by MS are given as:

$$\omega_3^2 = \frac{1}{8m}\left(a_{10} + a_{11} + a_{12}\sin\left(\frac{2\pi\omega_2}{\omega_1}\right) + a_{13}\sin\left(\frac{4\pi\omega_2}{\omega_1}\right) + a_{14}\sin\left(\frac{6\pi\omega_2}{\omega_1}\right)\right),$$

$$\omega_4^2 = \frac{1}{a_{15}}\left(a_{16}\sin\left(\frac{2\pi\omega_1}{\omega_2}\right) + a_{17}\sin\left(\frac{4\pi\omega_1}{\omega_2}\right)\right),$$

$$\mu_3 = a_{18}\sin\left(\frac{2\pi\omega_4}{\omega_3}\right),\ \ \mu_4 = a_{19}\sin\left(\frac{2\pi\omega_3}{\omega_4}\right),$$

where

$$a_{10} = 6k_4(C^2 + 2D^2) + 16k_3\ ,\ a_{11} = \frac{D\omega_3}{C\pi}\left(\frac{2\omega_4\left(-\omega_4^2(3k_4(4C^2 + D^2) + 4k_3)\right)}{9\omega_3^4 - 10\omega_3^2\omega_4^2 + \omega_4^4}\right),$$

$$a_{12} = \frac{D\omega_3}{C\pi}\left(\frac{2\omega_4\left(3\omega_3^2(28C^2k_4 + 9D^2k_4 + 12k_3)\right)}{9\omega_3^4 - 10\omega_3^2\omega_4^2 + \omega_4^4}\right),\qquad a_{13} = \frac{D\omega_3}{C\pi}\left(3Dk_4\left(\frac{C(\omega_3^2 - 2\omega_4^2)}{\omega_3^2\omega_4 - \omega_4^2}\right)\right),$$

$$a_{14} = \frac{D\omega_3}{C\pi}\left(3Dk_4\left(\frac{2D\omega_4}{\omega_3^2 - 9\omega_4^2}\right)\right),\ \ a_{15} = 8\pi Dm\omega_3(\omega_3^4 - 10\omega_3^2\omega_4^2 + 9\omega_4^4),$$

$$a_{16} = -8C\omega_3^2\omega_4(k_3(\omega_3^2 - 9\omega_4^2) + 3D^2k_4(\omega_3^2 - 7\omega_4^2)),$$

$$a_{17} = D(\omega_3^2 - 9\omega_4^2)(4(2k_3 + 3C^2k_4)\pi\omega_3(\omega_3^2 - \omega_4^2) - 3C^2k_4\omega_4(-2\omega_3^2 + \omega_4^2)),$$

$$a_{18} = \frac{b_1}{m_1}\left(1 + \frac{D\omega_3\omega_4}{C\pi(\omega_3^2 - \omega_4^2)}\right)\ \ a_{19} = \frac{b_1}{m_1}\left(1 - \frac{C\omega_3\omega_4}{D\pi(\omega_3^2 - \omega_4^2)}\right).$$

References

[1] G. Chen, Applications of a generalized Galerkin's method to non-linear oscillations of two-degree-of-freedom systems, *Journal of Sound and Vibration*, Vol. 119, No. 2, pp. 225-242, 1987.

[2] M. Bayat, I. Pakar, Shahidi, Analysis of nonlinear vibration of coupled systems with cubic nonlinearity,, *Mechanika*, Vol. 17, No. 6, pp. 620-629, 2011.

[3] L. Cveticanin, Vibrations of a coupled two degree-of-freedom system, *Journal of Sound and Vibration*, Vol. 247, No. 2, pp. 279-292, 2001.

[4] L. Cveticanin The motion of a two-mass system with non-linear connection, *Journal of Sound and Vibration*, Vol. 252, No. 2, pp. 361-369, 2002.

[5] S. Telli, O. Kopmaz, Free vibrations of a mass grounded by linear and non-linear springs in series, *Journal of Sound and Vibration,* Vol. 289, pp. 689-710, 2006.

[6] A. D. Dimarogonas, S. Haddad, 1992, *Vibration for Engineers,* Prentice-Hall, Englewood Cliffs, New Jersey

[7] M. T. Ahmadian, M. Mojahedi, H. Moeenfard, Free vibration analysis of a nonlinear beam using homotopy and modified Lindstedt-Poincaré methods, *Journal of Solid Mechanics,* Vol. 1, No. 1, pp. 29-36, 2009.

[8] Z. Guo, A. Y. Leung, H. X. Yang, Iterative homotopy harmonic balancing approach for conservative oscillator with strong odd-nonlinearity, *Applied Mathematical Modelling,* Vol. 35, pp. 1717-1728, 2001.

[9] J.-H. He, Homotopy perturbation technique, *Computer Methods in Applied Mechanics and Engineering,* Vol. 178, pp. 257-262, 1999.

[10] H. M. Sedighi, K. H. Shirazi, Dynamic pull-in instability of double-sided actuated nano-torsional switches, *Acta Mechanica Solida Sinica,* Vol. 28, No. 1, pp. 91-101, 2015.

[11] G. M. Ismail, M. Abul-Ez, N. M. Farea, N. Saad, Analytical approximations to nonlinear oscillation of nanoelectro-mechanical resonators, *The European Physical Journal Plus,* Vol. 134, pp. 47, 2019.

[12] J.-H. He, Variational iteration method-some recent results and new interpretations, *Journal of Computational and Applied Mathematics,* Vol. 207, No. 1, pp. 3-17, 2007.

[13] J.-H. He, A coupling method of a homotopy technique and a perturbation technique for non-linear problems, *International Journal of Non-Linear Mechanics,* Vol. 35, pp. 37-43, 2000.

[14] G. M. Ismail, M. Abul-Ez, M. Zayed, H. Ahmed, M. El-Moshneb, Highly accurate analytical solution for free vibrations of strongly nonlinear Duffing oscillator, *Journal of Low Frequency Noise Vibration and Active Control,* Vol. 41, No. 1, pp. 223–229, 2022.

[15] T. S. Amer, A. A. Galal, Vibrational dynamics of a subjected system to external torque and excitation force, *Journal of Vibration and Control,* Vol. 0, No. 0, pp. 1–14, 2024.

[16] K. Johannesen, The Duffing oscillator with damping for a softening potential, *International Journal of Applied and Computational Mathematics,* Vol. 3, pp. 3805–3816, 2017.

[17] A. H. Salas, S. A. El-Tantawy, On the approximate solutions to a damped harmonic oscillator with higher-order nonlinearities and its application to plasma physics: Semi-analytical solution and moving boundary method, *European Physical Journal Plus,* Vol. 135, No. 10, pp. 1–17, 2020.

[18] Y. Wu, Y.-P. Liu, Residual calculation in He's frequency–amplitude formulation, *Journal of Low Frequency Noise, Vibration and Active Control,* Vol. 40, No. 2, pp. 1040–1047, 2021.

[19] Z. F. Ren, G. F. Hu, He's frequency-amplitude formulation with average residuals for nonlinear oscillators, *Journal of Low Frequency Noise, Vibration and Active Control,* Vol. 38, pp. 1050–1059, 2019.

[20] N. Qie, W.-F. Houa, J.-H. He, The fastest insight into the large amplitude vibration of a string, *Reports in Mechanical Engineering,* Vol. 2, No. 1, pp. 1–5, 2020.

[21] J.-H. He, Amplitude–frequency relationship for conservative nonlinear oscillators with odd nonlinearities, *International Journal of Applied and Computational Mathematics,* Vol. 3, pp. 1557–1560, 2017.

[22] G. M. Ismail, G. M. Moatimid, M. I. Yamani, Periodic solutions of strongly nonlinear oscillators using He's frequency formulation, *European Journal of Pure and Applied Mathematics,* Vol. 17, No. 3, pp. 2154-2171, 2024.

[23] G. M. Moatimid, T. S. Amer, Dynamical system of a time-delayed φ6 -Van der Pole oscillator: A non-perturbative approach, *Scientific Reports,* Vol. 13, pp. 11942, 2023.

[24] G. M. Moatimid, T. S. Amer, Y. Y. Ellabban, A novel methodology for a time-delayed controller to prevent nonlinear system oscillations, *Journal of Low Frequency Noise, Vibration and Active Control,* Vol. 43, No. 1, pp. 525-542, 2024.

[25] G. M. Moatimid, T. S. Amer, A. A. Galal, Studying highly nonlinear oscillators using the non-perturbative methodology, *Scientific Reports,* Vol. 13, pp. 20288, 2023.

[26] G. M. Moatimid, A. T. El-Sayed, H. F. Salman, Different controllers for suppressing oscillations of a hybrid oscillator via non-perturbative analysis, *Scientific Reports,* Vol. 14, No. 1, pp. 307, 2024.

[27] G. M. Moatimid, M. A. Mohamed, K. Elagamy, Nonlinear Kelvin-Helmholtz instability of a horizontal interface separating two electrified Walters' B liquids: A new approach, *Chinese Journal of Physics,* Vol. 85, pp. 629-648, 2023.

[28] G. M. Moatimid, A. Sayed, Nonlinear EHD stability of a cylindrical interface separating two Rivlin-Ericksen fluids: A Novel analysis, *Chinese Journal of Physics,* Vol. 87, pp. 379–397, 2024.

[29] G. M. Moatimid, Y. M. Mohamed, A novel methodology in analyzing nonlinear stability of two electrified viscoelastic liquids, *Chinese Journal of Physics,* Vol. 89, pp. 679-706, 2024.

[30] G. M. Moatimid, Y. M. Mohamed, A novel methodology in analyzing nonlinear stability of two electrified viscoelastic liquids, *Physics of Fluids,* Vol. 36, pp. 024110, 2024.

[31] G. M. Moatimid, D. M. Mostafa, M. H. Zekry, A new methodology in evaluating nonlinear Eelectrohydrodynamic azimuthal stability between two dusty viscous fluids, *Chinese Journal of Physics,* Vol. 90, pp. 134–154, 2024.

[32] G. M. Moatimid, D. M. Mostafa, Nonlinear stability of two superimposed electrified dusty fluids of type Rivlin-Ericksen: Non-perturbative approach, *Partial Differential Equations in Applied Mathematics*, Vol. 10, pp. 100745, 2024.

[33] G. M. Moatimid, M. A. Mohamed, K. Elagamy, Insightful inspection of the nonlinear instability of an azimuthal disturbance separating two rotating magnetic liquid columns, *The European Physical Journal Plus*, Vol. 139, pp. 590, 2024.

[34] G. M. Moatimid, T. S. Amer, A. A. Galal, Inspection of some extremely nonlinear oscillators using an inventive approach, *Journal of Vibration Engineering & Technologies,*, 2024.

[35] J.-H. He An improved amplitude-frequency formulation for nonlinear oscillators, *International Journal of Nonlinear Sciences and Numerical Simulation,* Vol. 9, pp. 211–212, 2008.